Seasonal and developmental stage changes in exudate carbohydrate content shape the kelp microbiome

Chance J. English[*1,2], *Meenakshi Manoj*[1], *Lillian C. Henderson*[1], *Keri Opalk*[1], *Craig A. Carlson*[1,3]

1. Marine Science Institute, University of California Santa Barbara, CA, USA
2. Earth Research Institute, University of California, Santa Barbara, CA, USA
3. Department of Ecology, Evolution and Marine Biology, University of California Santa Barbara, CA, USA

* Corresponding author: Chance J. English

Email: cje@ucsb.edu

(951) 286-8416

Key Words: microbiome, macroalgae, dissolved organic carbon, carbohydrates, planctomycetota, alginate, fucoidan

Author Contribution Statement

CJE and CAC conceptualized the research. CJE collected material for and led the research. CJE, MM, LCH,and KO collected and analyzed data or performed laboratory measurements. CJE, MM, LCH ,KO, and CAC contributed to interpreting the results and writing/editing the manuscript. CAC and CJE acquired funding for the research.

Abstract

Photoautotrophs release a large amount of their fixed carbon as exudates, which shapes their immediate environment, including the composition of their microbiome. Here we evaluated the microbiome and exudate composition of *Macrocystis pyrifera* (giant kelp), a globally distributed foundation species, in response to seasonal nutrient availability and developmental stage. We combine 16S rRNA amplicon analysis of the giant kelp microbiome with carbohydrate monomer analysis of kelp exudates to examine microbe-exudate relationships. We found significant differences in the microbiome and exudate composition between seasons and developmental stages of giant kelp. Higher tissue-nitrogen content in the spring coincided with elevated amounts of glucosamine, a nitrogen-containing sugar, in giant kelp exudates, while senescence led to the shedding of mannuronic acid, an alginate indicator. The release of glucosamine and fucose-rich exudates was correlated with an increase in the relative abundance of bacteria within the Planctomycetota phylum, whereas mannuronic acid-rich exudates coincided with an increase in the relative abundance of members of the Flavobacteria and Gammaproteobacteria lineages. We investigated putative carbohydrate-microbe relationships by isolating a member of the Planctomycetota phylum from the surface of giant kelp. We demonstrate that the growth of this isolate on fucoidan and *N*-acetyl glucosamine, but not alginate reflects the observed relative abundance of this clade in the kelp microbiome in response to variable carbohydrate exudation. This suggests a key role of kelp mucilage carbohydrate composition in structuring its microbiome as has been observed for other organisms such as corals and within the human gut.

Introduction

Primary producers such as plants and macroalgae have evolved in environments surrounded by microorganisms, and in many cases, associated microbes can improve the fitness and growth of the host through defense or nutrient acquisition [1–4]. A growing body of evidence indicates that autotrophic organisms regulate their microbiome by exuding metabolites that promote microorganism growth or inhibit the growth of pathogens [5, 6]. The exudate and host-microbe associations are dynamic and can vary in response to the host's developmental stage and abiotic stressors [7, 8]. Unraveling the relationship between host physiology, exudate composition, and the microbiome structure can provide a mechanistic understanding of the establishment and function of the microbiome of primary producers.

Carbohydrates, including simple sugars, disaccharides and complex polysaccharides are typically the dominant organic material exuded by primary producers [9, 10]. The active exudation of carbon-rich organic matter by organisms was originally proposed as an "overflow" mechanism that allowed photosynthesis to continue when light and nutrients needed for biosynthesis became uncoupled [11, 12]. More recently, it has been proposed that the exudation of carbohydrate-rich material can also serve to prevent the attachment of pathogens [6], promote the growth of beneficial microbial partners [8, 13] or aid in the transport of energy and nutrients to the organism [14]. The potential role of carbohydrate exudation in shaping microbiomes is evidenced in studies of corals that reveal significant correlations between the host's exuded mucus sugar content and the relative abundance of certain microbial taxa [15, 16]. The composition of exuded

carbohydrates by corals is species-specific [17, 18] and varies in response to abiotic factors such as temperature [15]. While these relationships are established for corals, the role of carbohydrate exudation in shaping the microbiome has yet to be evaluated for important foundation species such as kelps.

Kelp forests are critical marine habitats that occupy 43% of the world's coastline [19]. In addition to their contributions to biodiversity [20] and global economies [21], it is hypothesized that kelps contribute to carbon sequestration through the export of dissolved organic carbon (DOC) and detrital particulate carbon [22–24]. In this context, the decline of kelp forests [25] due to stressors such as ocean warming is a serious threat to ecosystem function, marine carbon cycling, and economies. This has prompted calls for large-scale intervention through natural kelp forest restoration [26] or aquaculture to offset these losses and increase current production yields [27]. Therefore, identifying and understanding the underlying factors for kelp health and resilience is of critical importance for monitoring, management, and restoration of these ecosystems, their services, and the economies dependent on kelp.

Decades of research have focused on understanding the impact of environmental factors such as light, nutrients, wave disturbance, and temperature on kelp growth [28–32]. In temperate coastal areas, such as California, kelp growth rates and physiology are influenced by seasonal nitrate availability. Low seawater nitrate concentrations (NO_3^{-1} < 1μM) throughout the summer and fall result in elevated tissue carbon to nitrogen ratios and when tissue nitrogen content falls below 1% of dry mass, kelp survival can become compromised [32]. In comparison to abiotic factors, less is known about how the kelp

microbiome affects kelp growth and resilience, although there is a growing appreciation of role of the microbiome in kelp health and resistance to disease [33, 34]. Several studies demonstrate that kelp harbor a microbiome that is distinct from the surrounding seawater [35–37] and meta- and whole genome analysis of kelp microbiomes suggest potential positive interactions, such as antibacterial and antiherbivore defense, or vitamin acquisition [38–40], between kelp and specific microbial lineages such as Planctomycetota. Further, there are significant associations between environmental conditions (i.e. temperature, nutrients), the physiological condition of kelp, its productivity, and its microbiome composition [41–43]. However, the underlying mechanisms between kelp physiology and microbiome composition are unresolved, although previous studies suggest exudate composition, environmental perturbations, or the interaction between the two may be important [44–46].

In this study, we aimed to understand how the composition of kelp exudates shapes the microbiome of *Macrocystis pyrifera*, hereafter giant kelp. We hypothesized that abiotic factors (nitrogen availability) and developmental stage would alter the chemical composition of kelp exudates and that these altered chemical profiles would shape the giant kelp microbiome. We sampled tagged cohorts of giant kelp fronds to track the development of their microbiome across developmental stages and between the warm, nitrate depleted summer and nitrate replete spring upwelling periods. Simultaneous measurements of exudate carbohydrate composition and 16S rRNA gene analysis were employed to identify microbe-exudate associations. We observed significant correlations between abundant microbial taxa and the carbohydrate content of giant kelp exudates. To

test some of these associations, we isolated a member of the Planctomycetota phylum, a dominant kelp-associated bacterial group. Using whole genome sequencing, phylogenetic analysis and growth assays, we demonstrate that the carbohydrate substrate preferences of this clade reflect its relative abundance patterns in the kelp microbiome. This work suggests an important role for mucilage carbohydrate composition in shaping the kelp microbiome.

Methods

Sampling, kelp blade age and developmental stage, and environmental variables

Giant kelp blades were sampled from two tagged cohorts at Mohawk Reef (34º 23.6600' N, 119º 43.8000' W) in the Santa Barbara Channel, CA, USA in the summer of 2023 and spring of 2024. Cohorts were tagged by placing a cable tie around the stipe 2 m back from the apical meristem of 100-200 growing fronds. At intervals of 2-3 weeks, single blades (6 – 32 g wet weight) from 6 random fronds were sampled to measure their tissue nitrogen (tissue-N), exudate carbohydrate composition and microbiome. The developmental stage of kelp blades was categorized as either "mature" or "senescent" if they were younger than or older than 50 days old, respectively [29]. Blades were collected in the morning (08:00-10:00) and transported in a plastic cooler filled with ambient seawater to a near-shore laboratory, where they were incubated in 10 L acrylic tanks filled with filtered (0.2 µm) seawater. Incubations were started between 10:00-12:00 and maintained at *in situ* temperature (Summer: 17-19 ºC, Spring: 12-14 ºC) using a temperature-controlled water bath for 6-9 hours. Incubation tanks were equipped with

136 magnetic stir bars to maintain water circulation. Light levels were adjusted every 2-3 hours,
137 decreasing from saturating intensity (1140-1517 µmol photons m^{-2} s^{-1}) to darkness (0 µmol
138 photons m^{-2} s^{-1}) to simulate the transition from day to night. Duplicate DOC (n = 84) and
139 one hydrolyzable carbohydrate (n = 42) sample were collected by siphon at the beginning
140 and end of each incubation and filtered through pre-combusted glass-fiber filters
141 (Whatman GF-75, 0.3 µm nominal pore size). Following their incubation, kelp blade tissue-
142 N was sampled as a measure of nitrogen stress and developmental stage. For tissue-N
143 analysis, giant kelp blades were scraped cleaned of epibionts with a metal spatula, dried
144 at 60 ^{o}C for three days and then ground to a fine powder before analysis of a 10 mg
145 subsample with an Exeter Analytical CE-440 CHN/O/S elemental analyzer.
146 Environmental conditions at Mohawk Reef during our study were evaluated using
147 bottom temperature data collected by the Santa Barbara Channel Long-Term Ecological
148 Research program [47]. Average daily temperature was calculated from submersible
149 temperature loggers at Mohawk Reef. Nitrate concentrations were calculated from
150 temperature using an exponential "T2N" relationship derived from an inshore temperature
151 and nitrate dataset [48] (Supplemental Figure. 1).
152
153 *Exudate DOC, carbohydrate content and composition*
154 Dissolved organic carbon (DOC) analysis was carried out following established
155 protocols [49]. Briefly, duplicate DOC samples were taken from at beginning and end of
156 each incubation, filtered through pre-combusted 25 mm GF-75 into pre-combusted 40 ml

157 EPA vials with PTFE lined caps, acidified to pH < 3 with the addition of 60 µl of 4N HCl and
158 analyzed using a Shimadzu TOC-V or TOC-L.
159 Dissolved carbohydrate samples were taken alongside DOC samples and stored
160 frozen at -20ºC. Exudate carbohydrate content was measured by high-performance anion
161 exchange chromatography with pulsed amperometric detection (HPAEC-PAD). We
162 followed established dialysis and HPAEC-PAD gradients [50] . Briefly, samples were
163 dialyzed using Spectra/Por 7 tubing (1000 Da) against ultrapure water and then hydrolyzed
164 in duplicate for 20 hours at 100°C in 0.4 M HCl then neutralized under a flow of N_2 gas.
165 Samples were run on a DIONEX ICS5000+ and sugars were separated using a Carbopac
166 PA10 column (4x250mm) with a Carbopac PA10 guard column (4x50mm). Neutral and
167 amino sugars were eluted with 18mM NaOH followed by 100mM NaOH/200mM Na-
168 Acetate to elute acidic sugars. The system was calibrated using a common standard sugar
169 mix [17, 51] dissolved in ultrapure water containing fucose (1mM), rhamnose (1mM),
170 arabinose (1mM), galactosamine (0.25 mM), glucosamine (0.25 mM), galactose (1mM),
171 glucose (1mM), mannose+xylose (2 mM), galacturonic acid (1 mM), glucuronic acid (1 mM)
172 and mannuronic acid (0.5 mM). Linearity of the calibration curves were observed for
173 concentrations ranging from 10nM-1µM. In our dissolved carbohydrate samples, we
174 observed glucose and mannose+xylose contamination due to leaching from the
175 Spectra/Por 7 dialysis tubing, so these sugars were removed from subsequent analysis.
176 Previous studies demonstrate these sugars are not substantial components of
177 carbohydrates released by brown macroalgae [17, 52].

178 Principal component analysis was used to visualize changes in the composition of
179 hydrolyzable sugar monomers in giant kelp exudates. Sugars were normalized to molar
180 percentages (mole%) relative to other sugars. Statistical analysis of the differences in the
181 composition of the carbohydrates released by giant kelp between the two seasons and
182 developmental stages was evaluated by PERMANOVA using the *adonis* function in R (vegan
183 2.7-1) [53] on the scaled mole% of individual sugar monomers.
184
185 *Microbiome DNA extraction, 16S rRNA gene sequencing & amplicon analysis*
186 Following their incubation, but before their preparation for tissue-nitrogen analysis,
187 kelp blades were rinsed with 0.1 µm filtered sterilized seawater and sampled across the
188 entire surface by scraping with sterile cotton-tip swabs (Puritan®) for 30 seconds. Swabs
189 were placed in sterile 2 ml cryogenic tubes and frozen at -80 ºC. DNA samples were lysed
190 in sucrose lysis buffer (750 mM Sucrose, 20 mM EDTA, 400 mM NaCl, 50 mM Tris-HCl, pH =
191 8.0) with 1% SDS and 0.2 mg mL^{-1} proteinase-K at 37ºC for 30 minutes for cell lysis and
192 protein digestion, then at 55ºC for 30 minutes to complete the lysis and degradation of
193 cellular components. DNA was purified using the phenol-chloroform method [54]. For
194 amplification, we targeted the V4 region of the 16S rRNA gene using the 515F-Y (5'-
195 GTGYCAGCMGCCGCGGTAA-3') and 806RB (5'- GGACTACNVGGGTWTCTAAT-3') primers
196 (predicted 84% coverage of 16S rRNA sequences; SILVA TestPrime 1.0) with custom
197 adaptors [55]. PCR was carried out in 25 µL reactions with 12.5 µL KAPA Robust Hotstart
198 ReadyMix (final concentrations: 0.2 mM each dNTP, 1U DNA Polymerase, 2mM $MgCl_2$), 1uL
199 each of the forward and reverse primers (final concentration: 0.4 µM each), 2µL of bovine

200 serum albumin (final concentrationl: 1.6 μg μL^{-1}), 6.5 μL of PCR-grade water and 2μL of
201 sample DNA and cycled for 3 minutes at 95 ºC, followed by 30 cycles of 30 seconds at 95
202 ºC, 30 seconds at 57 ºC and one minute at 72 ºC, ending with 10 minutes at 72 ºC. Four
203 negative controls (PCR-grade water) and two mock community samples were included in
204 the PCR run for quality control. Following PCR, amplified DNA was quantified (Qubit,
205 Thermo Fisher) and manually normalized by pooling equal nmol amounts of DNA from
206 each PCR reaction well. Pooled DNA was concentrated using Amicon® Ultra 0.5mL 30K
207 centrifugal filters (Millipore) then non-target DNA bands were removed by gel
208 electrophoresis and extraction. Samples were sequenced on an Illumina MiSeq PE250 and
209 demultiplexed, with zero barcode/index mismatches allowed, at the University of
210 California, Davis DNA Technologies Core.
211 Demultiplexed raw sequence reads were quality checked and processed using
212 DADA2 [56] in R. Forward and reverse reads were trimmed to 240 and 150 bp, respectively.
213 Trimmed and error corrected reads were dereplicated and pair-end reads were merged
214 and assigned taxonomy using the SILVA database [49; v138.1 with species]. In all samples,
215 amplicons identified as mitochondria (0-100 reads, mean = 18 reads) or chloroplasts (143-
216 20,725 reads, mean = 3,216 reads) were removed. PCR-water and mock community
217 controls were checked to confirm consistent amplification and lack of contamination and
218 then removed from further analysis (Supplemental Data 1). Quality filtering of chimeric
219 sequences or sequences with ambiguous bases resulted in 4.4×10^6 sequences from 54
220 samples. Samples had a read depth from 25,077 to 106,379 sequences, averaging 81,976
221 and were not rarefied for further analysis [58]. We analyzed differences in microbially

222 community composition on kelp blades by season (summer vs. spring) and developmental
223 stage (mature vs. senescent).
224 For multivariate analysis, singleton and doubleton amplicon reads were removed
225 and remaining amplicon sequence variants (ASVs) were converted to relative abundances
226 and normalized using a variance stabilizing transformation. For beta diversity calculations,
227 samples were assigned NMDS scores based on Bray-Curtis dissimilarities using the
228 *metaMDS* function in phyloseq [59] and differences in community composition between
229 seasons and developmental stages were tested using a PERMANOVA with the *adonis*
230 function in the R [53] . For Shannon diversity calculations, performed with phyloseq,
231 singleton and doubleton amplicons were not removed. Significant differences in the mean
232 relative abundances of amplicons by season and developmental stage were evaluated
233 using the "DEseq2" package in R [60]. Differentially abundant ASVs were those that
234 displayed a log2 fold-change >1.5 between developmental stage or season and a
235 significant false discovery rate (FDR)-adjusted p-value (<= 0.01).
236 To identify relationships between the giant kelp microbiome and the exudate
237 carbohydrate composition we used hierarchical clustering of Spearman's rank
238 correlations between the relative abundance of significantly differentially abundant ASVs
239 and the mole% of sugar monomers simultaneously released by giant kelp blades. This
240 clusters ASVs based on their degree of correlation with the sugar content of kelp exudates
241 and allowed us to identify positive or negative microbe-carbohydrate relationships.
242 Hierarchical clustering was arranged using Ward's minimum variance method (squared
243 Euclidean distance) with the *pheatmaps* [61] package in R.

244

245 *Planctomycetota cultivation, genome sequencing & growth on model carbohydrates*

246 We enriched and isolated a strain of Planctomycetota following the suggestions of
247 Lage & Bondoso (2012) and Wiegand et al., (2020) [62, 63]. Agar plates were prepared with
248 0.1 µm filtered seawater with 1% agar. Seawater was autoclaved with agar then
249 supplemented with 1 ml L^{-1} vitamin solution (Biotin: 2 mg L^{-1}, Folic acid: 2 mg L^{-1},
250 Pyridoxamine-HCl: 10 mg L^{-1}, Thiamine-HCl x $2H_2O$: 5 mg L^{-1}, Riboflavin: 5 mg L^{-1}, Nicotinic
251 acid: 5mg L^{-1}, D-ca-pantothenate: 5 mg L^{-1}, Cyanocobalamine: 0.1 mg L^{-1}, p-Aminobenzoic
252 acid: 5 mg L^{-1}, Lipoic acid: 5mg L^{-1}, KH_2PO_4: 900 mg L^{-1}) and 1ml L^{-1} trace metal solution
253 (H_3BO_3: 2860 mg L^{-1}, $MnCl_2$ x $4H_2O$: 1810 mg L^{-1}, $FeCl_3$ x $6H_2O$: 316 mg L^{-1}, $ZnSO_4$ x $7H_2O$: 222
254 mg L^{-1}, Na_2MoO_4 x $2H_2O$: 390 mg L^{-1}, $CuSO_4$ x 5 H_2O: 79 mg L^{-1}, $Co(NO_3)_2$ x $6H_2O$: 49 mg L^{-1}).
255 For a carbon and nitrogen source we added 10 ml of 5% *N*-acetyl glucosamine. To prevent
256 fungal growth and select for Planctomycetota, the medium was supplemented with 20 mg
257 L^{-1} of econazole nitrate, 200 mg L^{-1}ampicillin and 1 g L^{-1} streptomycin. Bacterial inoculum
258 was scraped from the surface of a giant kelp blade using a sterile swab for 30 seconds and
259 resuspended in sterile medium without agar. The cell suspension was filtered through a
260 5.0 µm filter and enumerated using a GUAVA easycyte HT flow cytometer (Millipore). To
261 each agar plate we added ~2000 cells. Cell suspensions were streaked across the agar
262 plates and incubated at 20 ^{o}C until colonies were formed. After 1 month, colonies showing
263 characteristics of Planctomycetota (pink pigmentation, budding cell growth) were selected
264 for restreaking. Candidate colonies were restreaked three times to ensure isolation and
265 then identified using 16S rRNA gene metabarcoding of the V4 region using the SILVA Ref NR

266 SSU r138.1 database. Whole-genome sequencing was performed on the Illumina NovaSeq
267 X Plus platform, producing 2 x 151 bp paired-end reads (Seqcenter, Pittsburgh, PA).
268 Trimmomatic (v0.39) and RQCFilter (BBTools v38.22) were used to remove low-quality or
269 short reads. Reads were assembled and annotated with SPAdes (v3.15.3) and Prokka
270 (v1.14.5), respectively, in the KBase platform [64]. Completion (99.93%) and
271 contamination (1.18%) was checked using CheckM v1.0.18. For phylogenetic analysis, 14
272 publicly available isolate genomes from the *Pirellulaceae* family were selected from
273 NCBI's GenBank database and compared to our assembled genome (Supplemental Data
274 2). The genome of *Planctomicrobium piriforme* from the Planctomycetota order
275 Planctomycetales was selected as the outgroup. A maximum-likelihood tree was
276 constructed with GToTree [65] using 74 bacteria marker genes and visualized using the
277 iTOL server. Carbohydrate-active enzymes associated with fucoidan and alginate
278 degradation were predicted for our isolate and reference isolates using a set of Hidden
279 Markov Models (HMMs) from the dbCAN2 CAZy collection using HMMER 3 software [66,
280 67]. Secondary metabolite production potential was analyzed using AntiSMASH [68].
281 We tested the ability of the *Rhodopirellula sp*. isolate to grow on model
282 carbohydrates in batch cultures. We prepared artificial seawater (ASW) as incubation
283 medium (0.42M NaCl, 0.029M Na_2SO_4, 0.01M KCl, 1mM KBr, 0.05mM H_3BO_3, 0.07mM
284 NaF,0.05M $MgCl_2$, 0.01M $CaCl_2$, 0.06mM $SrCl_2$, 2.5mM $NaHCO_3$). Medium salinity and pH
285 were adjusted to 33 ppt and 7.5, respectively and then autoclaved. Sterile ASW was
286 amended with 0.1 µm filter sterilized vitamin and trace metal solutions (described above,
287 1ml L^{-1}) and inorganic nutrients (10 mg L^{-1} NH_4Cl, 1 mg L^{-1} KH_2PO_4). Triplicate 50 ml

288 incubations were prepared for the following treatments: no amendment, *N*-acetyl
289 glucosamine (NAGA; 25 mg L^{-1}), alginate (25 mg L^{-1}), and fucoidan (25 mg L^{-1}). Because
290 commercially available fucoidan is typically contaminated, notably by alginate and
291 polyphenols [69, 70], we used ion exchange chromatography (IEX) to purify fucoidan
292 sourced from giant kelp (Sigma-Aldrich, product #F8065). Purification was performed using
293 a medium-scale IEX setup described by Sichert et al. (2021) [70]. The composition of the
294 purified fucoidan was checked by ^{1}H-^{13}C HSQC NMR and HPAEC-PAD (Supplemental
295 Figures 2, 3 & 4). Alginate (Sigma-Aldrich PHR1471) and NAGA (Fisher Scientific
296 ICN100068) were certified to be 88 and 100% pure, respectively. An isolate colony was
297 resuspended in sterile ASW without amended carbohydrates. After gently shaking for 20
298 minutes, the cell suspension was 5.0 µm filtered and enumerated using a GUAVA easycyte
299 HT flow cytometer (Millipore). Cells were added to incubation vessels at a concentration of
300 ~6.0×10^{4} cells ml^{-1}. For all treatments, triplicate control incubations without cells were
301 sampled to confirm sterility of the incubation media and carbohydrate amendments.
302 Incubations were monitored semi-daily by cell enumeration for nine days by flow
303 cytometry (GUAVA easycyte HT, Millipore).
304
305 **Results**
306 *Kelp physiological response to seasonal nitrate availability and developmental stage*
307 We observed variations in kelp developmental stage driven by seasonal nitrate
308 availability and age. In both seasons, rapid changes in physiology occurred after kelp
309 blades passed 50 days of age, which we use to demarcate the transition from maturity to

310 senescence. Across all samples, tissue-N ($g_{Nitrogen}/g_{Dry\ Weight}$*100) ranged from 0.63% to
311 3.7%. Mature kelp sampled in the spring had a significantly higher tissue-N content than
312 mature summer kelp due to higher seawater nitrate concentrations (Figure 1, Figure 2A;
313 Welch's t-test: $t = -22.6$, $df = 19.0$, $p < 0.001$). The average (±1 SD) tissue-N of mature kelp
314 blades in the summer and spring were 0.92 ± 0.08% and 2.6 ± 0.14%, respectively (Figure
315 2A). After entering the senescent phase, average (±1 SD) tissue-N decreased to 0.7 ±
316 0.06% and 2.1 ± 0.77% in the summer and spring, respectively (Figure 2A).
317
318 *Seasonal and developmental stage-driven changes in exudate carbohydrate composition*
319 Hydrolyzable carbohydrates averaged 10.3 ± 4.9% of giant kelp exudate carbon
320 across all incubations, regardless of season or age. We observed a significant difference in
321 the carbohydrate sugar content of kelp exudates between the mature and senescent
322 developmental stages (Figure 2B; PERMANOVA, $R^2 = 0.14$, $p < 0.001$) and between seasons
323 (PERMANOVA, $R^2 = 0.07$, $p = 0.006$). Differences in sugar content between developmental
324 stages were driven by the change in mole% of fucose and mannuronic acid (Figure 2B)
325 which made up, on average, 47% and 5% of the sugars exuded in the mature phase,
326 respectively and 32% and 33% of the sugars exuded in the senescent phase, respectively
327 (Supplemental Figure 5). Man-URA had the largest change in mole% of all sugars between
328 the mature (5%) and senescent (34%) phases. In mature kelp blade exudates, the molar
329 percentage of glucosamine increased significantly from summer (3%) to spring (13%),
330 demonstrating the largest seasonal change (Figure 2C; t.test, $p < 0.001$).
331

Microbe-Carbohydrate dynamics

Coincident with altered exudate carbohydrate composition, we observed significant differences in the giant kelp microbiome between seasons and developmental stages. In both seasons we observed a significant increase in bacterial diversity with age (Ordinary Least Squares regression; Spring: $R^2 = 0.82$, $p < 0.001$; Summer: $R^2 = 0.23$, $p = 0.01$) although the spring cohort had lower initial diversity (Figure 3A). Multivariate analysis demonstrated that the composition of giant kelp microbiome was significantly different between season (PERMANOVA, $R^2 = 0.26$, $p < 0.001$) and developmental stage (PERMANOVA, $R^2 = 0.18$, $p < 0.001$) and there was a significant interaction between season and developmental stage (Figure 3B; Two-way PERMANOVA, $R^2 = 0.10$, $p < 0.001$). Family level shifts between mature and senescent kelp were largely driven by a significant increase in *Flavobacteriacea*, and *Arenicellaceae*, *and Rhodobacteraceae* and a significant decrease in Granulosicoccaceae, *Pirellulaceae, and Hyphomonadaceae* (Figure 4, ANOVA, FDR-adjusted p-value < 0.05, Supplemental Table 1). Family level changes were less pronounced between seasons (Supplemental Figure 6, Supplemental Table 2). At the ASV level, we identified 371 unique taxa that varied significantly in relative abundance between season or developmental stage, most of which were from the phyla Actinobacteriota, Bacteroidota, Planctomycetota, Proteobacteria (Gammaproteobacteria in particular) and Verrucomicrobiota (FDR-adjusted p-values <0.01, DEseq2, Supplemental Data 2, 3). Of these 371 ASVs, 44 had a relative abundance > 1% in more than 10% of samples. We consider these 44 ASVs to be abundant and common microbial taxa in the giant kelp microbiome. Hierarchical clustering was used to identify

354 relationships between these 44 abundant ASVs and the mole% of sugars exuded by giant
355 kelp based on Spearman's rank correlation coefficients.

356 For 17 of the 44 ASVs there was at least one significant correlation (Spearman's
357 rank correlation, $\rho > 0.5$, FDR-adjusted $p < 0.05$, Supplemental Table 3 & 4) with the mole%
358 of a sugar in giant kelp exudates. These ASVs grouped into two clusters, primarily based on
359 their correlation with fucose, glucosamine, and mannuronic acid (Figure 5A). The first
360 cluster (Cluster A) included ASVs whose relative abundance was positively correlated with
361 the release of carbohydrates rich in fucose and/or glucosamine or negatively correlated
362 with mannuronic acid (Supplemental Table 3). Members of the family *Pirellulaceae* from
363 the phylum Planctomycetota accounted for 3 of the 6 ASVs in Cluster A. Cluster A also
364 contained two ASVs from the family *Granulosicoccaceae* in the phylum Proteobacteria
365 (Figure 5B).

366 The second cluster (Cluster B) was characterized by a significant positive
367 relationship between ASVs and the release of carbohydrates rich in mannuronic acid
368 and/or a negative correlation with the release of carbohydrates rich in fucose and/or
369 glucosamine (Supplemental Table 4). This cluster included members of the families
370 *Flavobacteriaceae, Cellvibrionaceae, Arenicellaceae, Trueperaceae, Thiotrichaceae and*
371 *Granulosicoccaceae*.

372

373 *Planctomycetota growth on model carbohydrates*

374 We cultivated a bacterial isolate from the surface of a giant kelp blade belonging to
375 the phylum Planctomycetota (family *Pirellulaceae,* genus *Rhodopirellula*) (Figure 6A & 6B)

that we used in subsequent growth assays on model carbohydrates. We confirmed the ability of *this Rhodopirellula sp*. to grow on different carbohydrates, including those from kelp (Figure 6C). We observed no growth in our sterile media controls, or the carbohydrate amended media without cells. In treatments with the the isolate added we observed no cell growth in unamended treatments. The isolate grew on both *N*-acetyl glucosamine and fucoidan, but not alginate.

Discussion

Nutrient availability and age shape kelp physiology

Giant kelp physiology between and within cohorts responded to seasonal nitrogen availability and age-related senescence. At our study site, giant kelp growth is primarily limited by inorganic nitrogen availability, which is depleted in the summer, but is replenished in the spring due to coastal upwelling (Figure 1) [71, 72]. Giant kelp adjusts to periods of low nitrogen availability by adjusting its tissue nitrogen content, resulting in elevated tissue C:N ratios [71] . In our study, the average percent tissue-N of mature giant kelp in the summer (0.91 ± 0.06%) was below the minimum value (0.98%) recorded in the SBC-LTER time-series of kelp at our study site, whereas the percent tissue-N in the spring was, on average (2.6 ± 0.14%), equal to the average for our study site (2.7 ± 0.8%) [72] .In this context, our summer sampling captured kelp in a period of nitrogen depletion (Tissue-N < 1%) which is suggested to result in diminished growth rates and kelp survival [32].

In addition to seasonal fluctuations in physiology, giant kelp undergoes progressive senescence, a rapid decline in developmental stage in response to age [73]. Our results

398 align with previous studies indicating that senescence occurs independently of
399 environmental conditions and begins when kelp tissue age exceeds approximately 50 days
400 [29]. These age-related physiological changes were associated with a decrease in tissue-N
401 (Figure 2A) and changes in the composition of dissolved carbohydrates released from giant
402 kelp (Figure 2B & 2C).
403
404 *Giant kelp microbiome composition*
405 The relative abundance of major epibiont bacterial families at different stages of
406 kelp development is broadly consistent with observations of kelp microbiomes over tissue
407 age and between healthy and stressed or senescent tissue (Figure 4) [35, 41, 42, 74, 75].
408 Likewise, the increase in diversity of the microbiome with age is consistent with previous
409 observations [74]; however, to our knowledge this is the first report of significantly lower
410 Shannon diversity in young kelp in the spring compared to the summer (Figure 3A). It has
411 been proposed that the kelp microbiome is established through environmental acquisition
412 over vertical transmission [76]. Therefore, exudates likely play a major role in the
413 establishment and transformation of the kelp microbiome. Kelps continuously shed and
414 replace tissue year-round [77] and factors that affect exudate composition, such as
415 nitrogen availability, may have consequences for the biofilm composition of new tissue, as
416 has been proposed for developing terrestrial plant rhizospheres [7].
417
418 *Exudate and microbiome composition dynamics*

419 Simultaneous changes in the carbohydrate composition of kelp exudates and
420 microbial taxa suggest an important role in exudate composition in shaping the kelp
421 microbiome. These associations further revealed that extrinsic factors, such as nitrogen
422 availability, and intrinsic factors such as development stage regulate the composition of
423 the giant kelp exudates. Notably, we observed an enrichment of glucosamine, a nitrogen-
424 containing sugar, in carbohydrates exuded by mature kelp in the spring compared to the
425 nitrogen-depleted kelp in the summer (Figure 1C). A similar pattern has been observed in
426 the root exudates of plants, whereby the addition of inorganic nitrogen results in the
427 enhanced release of nitrogen containing metabolites relative to roots grown under
428 nitrogen-limiting conditions. Baker et al., (2024) [7] found that the release of nitrogen-rich
429 metabolites by plant roots selected for a less diverse and unique microbial community
430 compared to plants grown in nitrogen-limited conditions, a pattern we also observed in the
431 kelp microbiome (Figure 2). Glucosamine is a common sugar in the mucus produced by
432 many organisms, including corals and humans [15, 18, 78], and has been shown to serve
433 an important role in regulating attachment and biofilm formation by bacteria [79, 80].
434 Because kelp exudates are constantly sloughed into the surrounding seawater, they must
435 be replaced to maintain their function in the extracellular matrix (mucilage). Therefore, the
436 cost of exuding nitrogen containing compounds that must be continuously replaced may
437 be too high to be maintained under nitrogen-depleted conditions experienced by giant kelp
438 in the summer.
439 Fucose was the most abundant sugar in the carbohydrates released by mature
440 giant kelp in both seasons, consistent with previous studies of brown macroalgae [17, 51,

441 52]. The presence of fucose in brown macroalgal exudates is due to the secretion of
442 fucoidan, a water-soluble, sulfated polysaccharide that is deposited onto the exterior of
443 the thallus through secretory canals to build the kelp's extracellular mucilage, which is
444 continuously sloughed into the surrounding seawater [81, 82]. Fucoidan lacks nitrogen
445 which may explain its consistent dominance in kelp exudates across a range of tissue-N
446 content. Several studies document the potential defensive properties of fucoidans [69, 79,
447 83] and its proposed defensive role is supported by its observed recalcitrance to bacterial
448 degradation [84].

449 In both seasons, there was an increase in the mole% of mannuronic acid as kelp
450 blades aged and senesced (Figure 1B). Mannuronic acid is an indicator of the macroalgal
451 polysaccharide alginate, which comprises up to half of kelp biomass [85]. Microbial taxa
452 positively correlated to the mole% of mannuronic acid included members of the family
453 *Flavobacteriaceae* and several Gammaproteobacteria, including one member of the family
454 *Thiotrichaceae* (Figure 5A, Cluster B). Flavobacteria and Gammaproteobacteria are
455 archetypal fast-growing carbohydrate degraders with adaptations to grow attached to
456 surfaces and are enriched in alginate and oligoalginate lyases [86–89]. Using DNA stable
457 isotope probing with ^{13}C-labeled alginate, Thomas et al., (2021) [86] demonstrated the
458 main consumers of alginate in coastal seawater were bacteria from the families
459 *Flavobacteriaceae*, *Alteromonadaceae*, *Thiotrichaceae* clades. The relative abundance of
460 *Flavobacteriaceae* and *Thiotrichaceae* in kelp biofilms is typically higher on stressed or
461 senescent kelp tissue [35, 75] as observed in this study (Figure 4), and in the early stages of
462 kelp biomass decay these groups dominate alginate hydrolysis [87]. From our

463 observations, we hypothesize that as kelp begins to senesce, the hydrolysis of insoluble
464 alginate polymers promotes the growth of alginate degraders whose hydrolytic enzymes
465 further solubilize kelp tissue into DOC. This dynamic would explain the enhanced
466 solubilization of kelp tissue with age that we observed in a complementary study [90].
467 The senescence-associated release of alginate is likely initiated by early alginate
468 degrading "pioneer" bacteria whose alginate lyases release alginate oligomers into the
469 environment, facilitating the growth of alginate "harvesters" and "scavengers" [91]
470 Notably, these potential alginate degraders were observed at low relevant abundance in
471 the mature kelp microbiome (Figure 5B), suggesting some process limited their growth
472 until kelp entered its senescent phase. The mechanisms of kelp senescence are not well
473 understood; however, senescence of giant kelp blades in both seasons occurred after 50
474 days of age, following linear decline in photosynthetic rates (see our complementary study
475 [90]), suggesting intrinsic regulation of senescence [92]; although, we cannot completely
476 rule out that associated bacteria contributed to senescence.
477
478 *Potential mechanisms behind carbohydrate-microbe associations*
479 Without further study of their native composition, we can only speculate about the
480 structure and function of the carbohydrates released by giant kelp. However, the role of
481 carbohydrates secreted to the outer membrane layers of animals and phytoplankton is
482 well established. For example, in bacterial biofilm formation, carbohydrates tethered to
483 the cell surface of a host serve as recognition sites for carbohydrate-protein binding
484 proteins (lectins) that act in concert with larger attachment proteins (adhesins). These

485 lectin-adhesin complexes mediate the attachment of bacteria, including pathogens to the
486 host surface [93]. In a model bacterium-diatom association, the lectin *Mp*PA14 exhibits a
487 strong binding affinity for fucose and *N*-acetyl glucosamine residues [79]. Guo et al., (2021)
488 demonstrated that *Mp*PA14 and the *Mp*PA14 lectin homolog from *Vibrio cholera* were
489 inhibited and unable to bind to diatom cells when exposed to high concentrations of free
490 fucose. A strong binding affinity of *Mp*PA14 was also observed for fucoidan, a fucose-rich
491 polysaccharide released by brown macroalgae. These data indicate a potentially
492 conserved defensive role of fucose-containing carbohydrates exuded by members of the
493 Stramenopile lineage, such as diatoms and kelps.

494 Giant kelp may release high concentrations of fucose-rich carbohydrates to disrupt
495 biofilm formation by potential pathogens. Indeed, all taxa from Cluster B (Figure 4A), which
496 includes several taxa associated with macroalgal tissue degradation, such as
497 Flavobacteria, exhibited a negative correlation with the fucose content of the exuded
498 carbohydrates (Spearman's ranked correlation, FDR-adjusted $p < 0.05$; Supplemental
499 Table 4). This was surprising, as previous metagenomic-based studies predict that
500 members of the Bacteroidetes phylum, especially *Flavobacteraceae*, are specialized to
501 degrade fucoidans [94, 95]. Therefore, other factors, in addition to carbohydrate substrate
502 preferences may contribute to the structuring of the kelp microbiome; possible factors
503 could be the production of secondary metabolites by Planctomycetota [63, 96] or the anti-
504 biofilm property of fucoidan [79]. Regarding the former, AntiSMASH analysis of our isolated
505 *Rhodopirellula* genome annotated two terpene biosynthetic gene clusters, two type I
506 polyketide synthases (PKS), one type III PKS, and hybrid type I PKS/terpene and type I/non

507 ribosomal peptide synthases (Supplemental Figure 7). This is consistent with other
508 isolates from the *Pirellulaceae* family [63] and suggests their abundances in kelp biofilms
509 may be due to a combination of their ability to degrade fucoidan (Figure 6C) and their
510 production of defensive secondary metabolites. Experiments to address secondary
511 metabolite production by this isolate are currently underway.

512 Glucosamine may serve as an important carbon and nitrogen source for the growth
513 of microbes beneficial to giant kelp. In the marine environment, glucosamine is more
514 commonly found in its acetylated form (*N*-acetyl glucosamine) [97]. Our carbohydrate
515 measurements require an acid hydrolysis step, which cleaves the acetyl group resulting in
516 glucosamine. Therefore, our glucosamine measurements reflect the contribution of both
517 *N*-acetyl glucosamine and glucosamine residues. The microbial taxa that positively
518 correlated with glucosamine included members from the family *Pirellulaceae* within
519 Planctomycetota, and the *Granulosicoccaceae* family of Proteobacteria (Cluster A, Figure
520 5A, Supplemental Table 3). Cultured strains of Planctomycetota such as *Pirellula* sp. strain
521 1 can metabolize *N*-acetyl glucosamine (NAGA) as their sole carbon and nitrogen source
522 [98], and in a comparison of 79 cultured members of Planctomycetota, *N*-acetyl
523 glucosamine was found to be the most efficient carbon source for their isolation [63].
524 Moreover, previous work suggests *N*-acetyl glucosamine may trigger biofilm formation by
525 some members of Planctomycetota, such as *Rhodopirellua baltica* [99].

526 Planctomycetes are dominant members of healthy macroalgal microbiomes [35,
527 42, 100] and it has been proposed they alter the composition of biofilms through the
528 production of secondary metabolites such as stieleriacines [96]. We demonstrate that a

529 *Rhodopirellula* strain, isolated from the surface of a giant kelp blade, can grow on fucoidan
530 and NAGA, but not alginate (Figure 6C). This carbohydrate substrate preference is
531 consistent with our observed correlations between the relative abundance of members of
532 the Planctomycetota family *Pirellulaceae* in the kelp microbiome and the sugar content of
533 giant kelp exudates (Figure 5A, Cluster A). Although only one isolate was tested in this
534 study, the ability for growth on fucoidan but not alginate is broadly consistent with the
535 metabolic potential of other isolated members of the family *Pirellulaceae* (Figure 6A).
536 Further, several recent studies also confirm that the isolates from the *Pirellulaceae* family
537 degrade fucoidan [38, 101]. We also note that even though some *Pirellulaceae* genomes,
538 including our isolate genome, contained copies of the alginate lyases PL6 or PL7, none
539 contain the oligoalginate lyases PL15 or PL17, which degrade oligoalginates into
540 monomers for metabolism (Figure 6A) [91]. We hypothesize that exudation of specific
541 carbohydrates, such as fucoidan serves to enrich their microbiome in commensal or
542 beneficial microbes such as Planctomycetota. Such carbohydrate-microbe synergy is
543 consistent with observations of plant rhizospheres, corals and the human gut [15, 78, 102–
544 104].
545

546 **Acknowledgments**

547 We thank all past and current members of the Santa Barbara Coastal LTER who
548 generated necessary background data for this study. We thank all Carlson lab members, A.
549 Santoro and D. Siegel for their constructive comments and discussion of the data and
550 manuscript. We thank P. Thieringer for his advice on whole genome assembly and

comparative genomics. This project was funded by the Department of Energy's Advanced Research Project Agency-Energy through award DE-AR0001559 to CAC, and the National Science Foundation's Santa Barbara Coastal LTER through award number OCE-1831937 to CAC. CJE and MM were additionally supported by the Worster Family Summer Research Fellowship awarded to CJE.

Data Availability

DNA sequence data are available in the National Center for Biotechnology Information Sequence Read Archive under PRJNA1256130. R scripts for analysis can be found at https://github.com/chance-english.

Figures

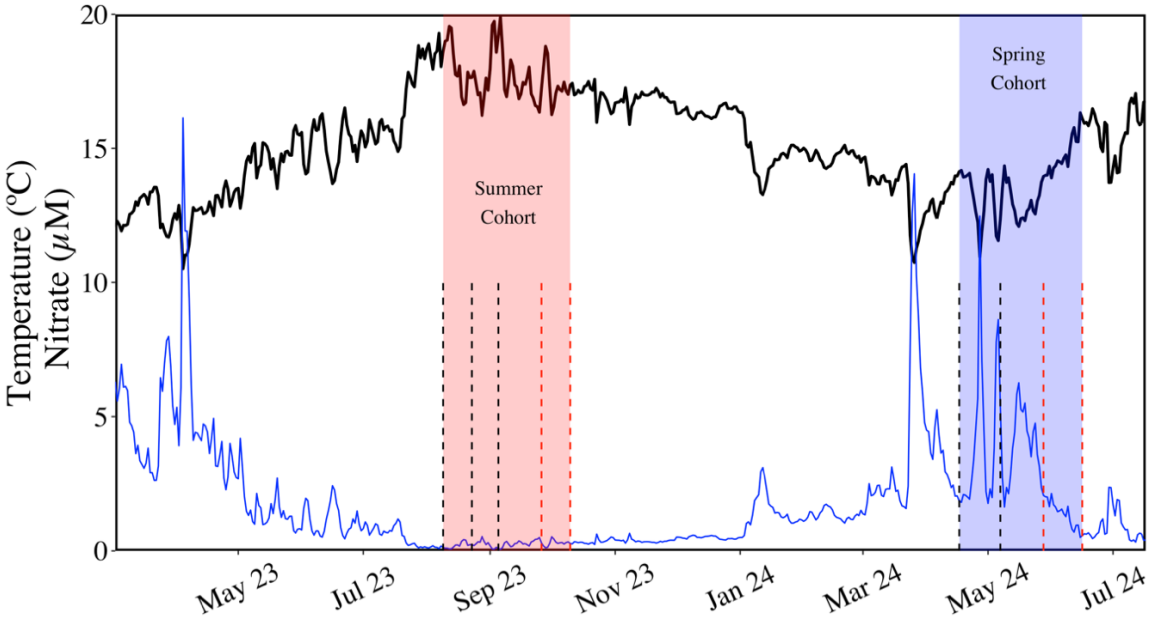

Figure 1. Mohawk Reef environmental conditions and sampling dates in this study. Daily average temperature (solid black line) and nitrate (solid blue line) concentrations between January 2023 and August 2024. Shaded red and blue regions show the sampling periods for the summer and spring cohorts used in this study, respectively. Vertical dashed lines extending from the x-axis mark the sampling dates within each cohort. The black and red color of the dashed lines indicate sampling of kelp that was in a mature (< 50 days) or senescent (> 50 days) development stage, respectively.

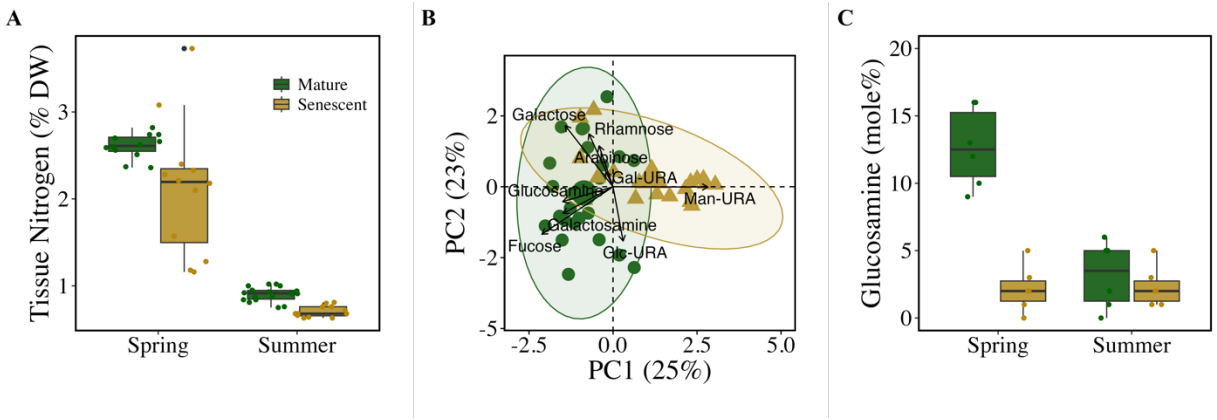

Figure 2. Seasonal and developmental stage changes in giant kelp physiology and exudate carbohydrate composition. (A) Giant kelp tissue nitrogen content as a percentage of dry weight (DW) between mature and senescent phase kelp in spring and summer. **(B)** Principle component (PC) analysis of giant kelp carbohydrate exudates as molar percentages between mature and senescent phase kelp. Ellipses represent 95% confidence regions between mature (green circles) and senescent (gold triangles) kelp exudates. Arrow lengths represent the strength of the correlation between each individual sugar monomer to the two principal components (PC1 & PC2) shown. Large symbols in center of the ellipses are the centroids. Sugar monomer names are overlayed next to arrows. Abbreviations: Glc-URA (glucuronic acid), Gal-URA (galacturonic acid), Man-URA (mannuronic acid). **(C)** Mole% of glucosamine in total moles of sugars exuded by giant kelp between developmental stages and seasons. Green and gold colors represent samples from mature and senescent kelp, respectively and are consistent for all three panels. Boxplots: The top and bottom border of each box represent the 25th and 75th percentiles, the horizontal line inside each box represents the median and the whiskers represent the range of the points (1.5*IQR) excluding outliers. Outliers are shown by black points outside the whiskers. Colored points show sample values for each boxplot.

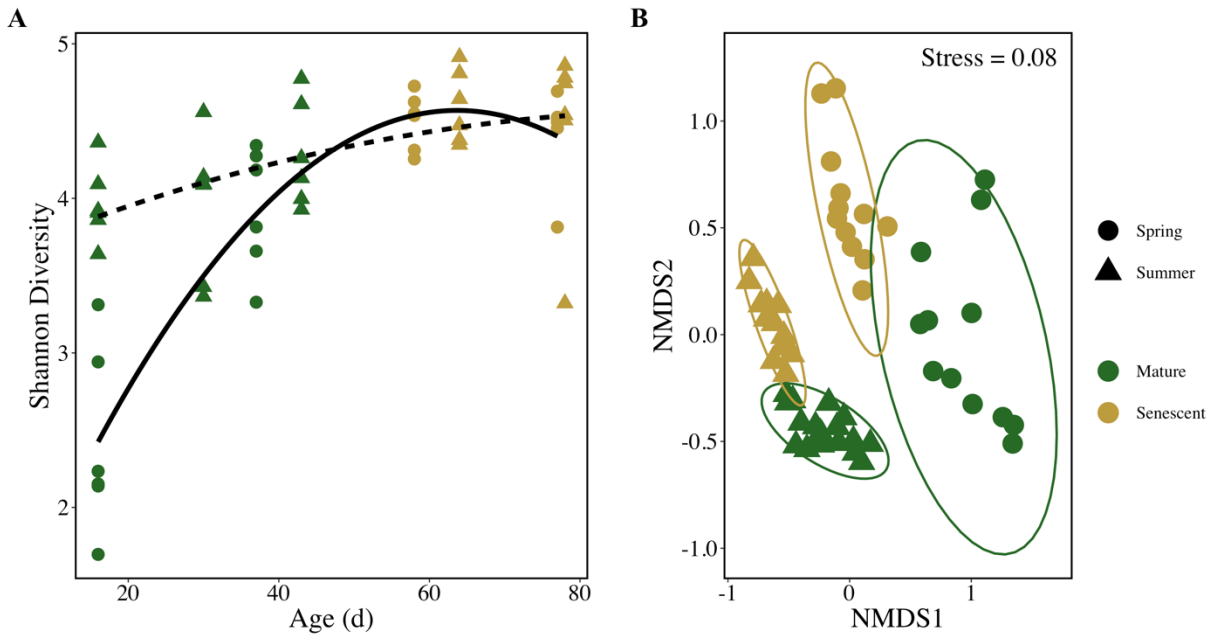

Figure 3. Giant kelp microbiome alpha and beta diversity between seasons and development stage. **(A)** Shannon diversity over age of the blade between spring (circles) and summer (triangles). Solid and dashed lines show the significant 2nd order polynomial relationship between the giant kelp microbiome Shannon diversity and age in the spring and summer cohorts, respectively. **(B)** NMDS plot showing significant difference in the microbial community composition between seasons and development stage. NMDS ordinations used Bray-Curtis dissimilarities from arcsine-transformed 16S rRNA amplicon relative abundances. The legend applies to both panels.

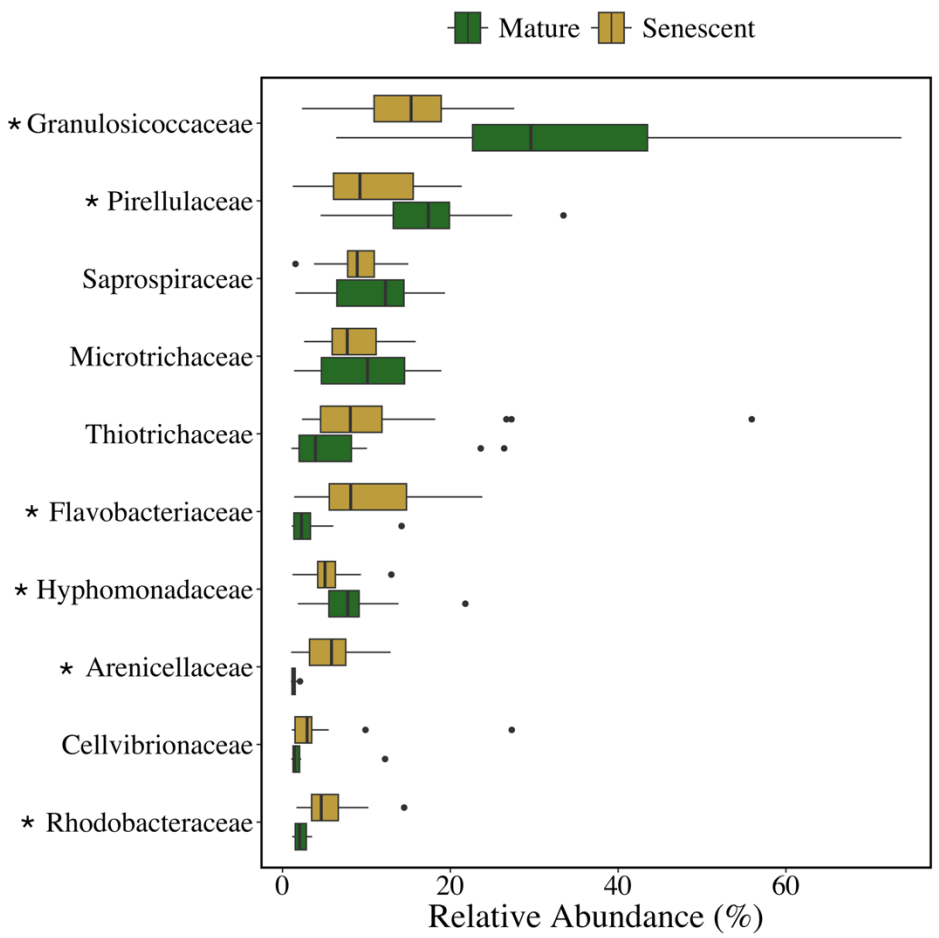

Figure 4. Relative abundance of bacterial clades at the family level on the surface of giant kelp blades between mature and senescent developmental stages. Shown are the top 10 families with a collective relative abundance > 1% during either developmental stage. The left and right border of each box represent the 25th and 75th percentiles, the vertical line inside each box represents the median and the whiskers represent 1.5*IQR. Outliers are shown by points beyond the whiskers. Asterisks next to family names indicate significant differences in the relative abundances between developmental stages (ANOVA, FDR-adjusted p-value < 0.05).

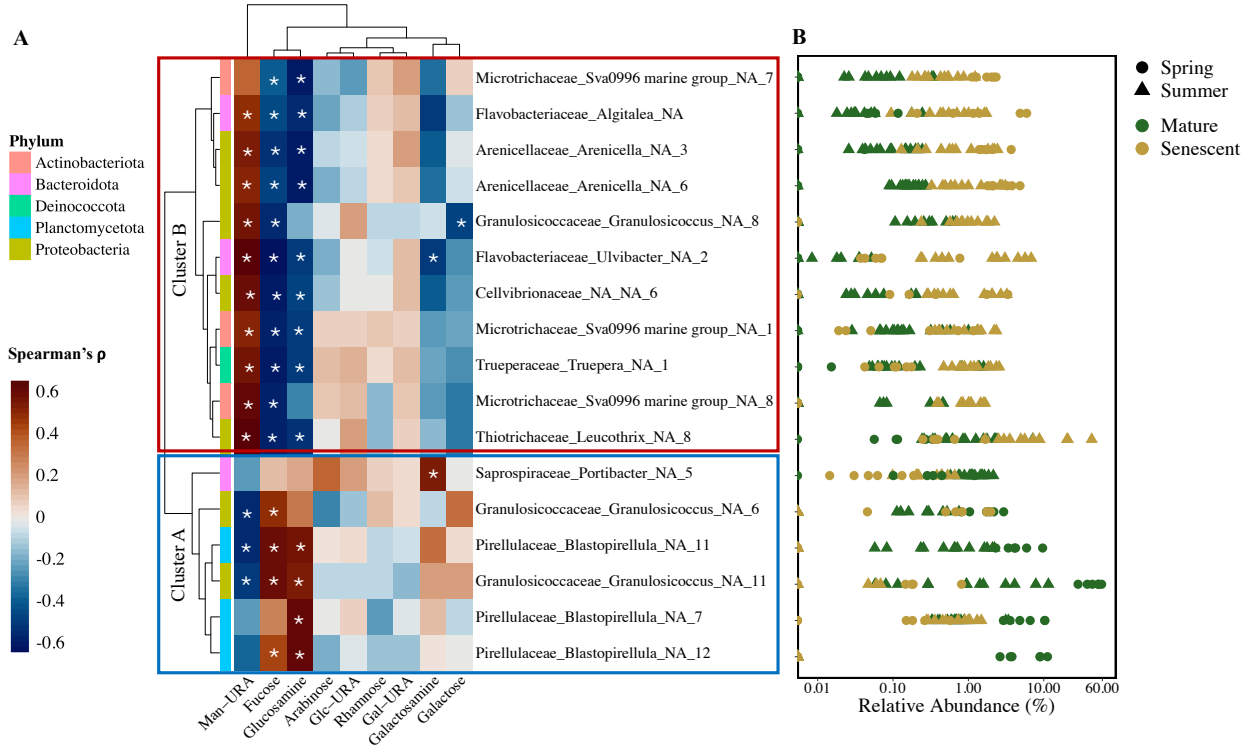

Figure 5. Abundant microbes are differentially correlated to the sugar content of giant kelp exudates. (A) Heatmap showing the Spearman's rank correlation coefficient between the relative abundance of differentially abundant ASVs (n = 17) with at least one significant positive or negative correlation (Spearman's rank correlation, $\rho > 0.5$, FDR-adjusted p-value < 0.05) with the mole% of a sugar monomer in giant kelp exudates. The strength and direction of the Spearman's ranked correlation are shown by the color ramp. Significant correlations are show by the white asterisk. Hierarchical clustering shows two main clusters of ASV-sugar correlations. Cluster A is shown in the blue rectangle, and Cluster B is shown in the red rectangle. The phylum of each ASV is shown by the row color at the tip of each branch. Abbreviations: Glc-URA (glucuronic acid), Gal-URA (galacturonic acid), Man-URA (mannuronic acid). **(B)** Range in the relative abundance of each differentially abundant taxa in all kelp microbiome samples across season and physiological state.

Season and physiological state of the kelp from which the sample was taken is shown by the point color and shape.

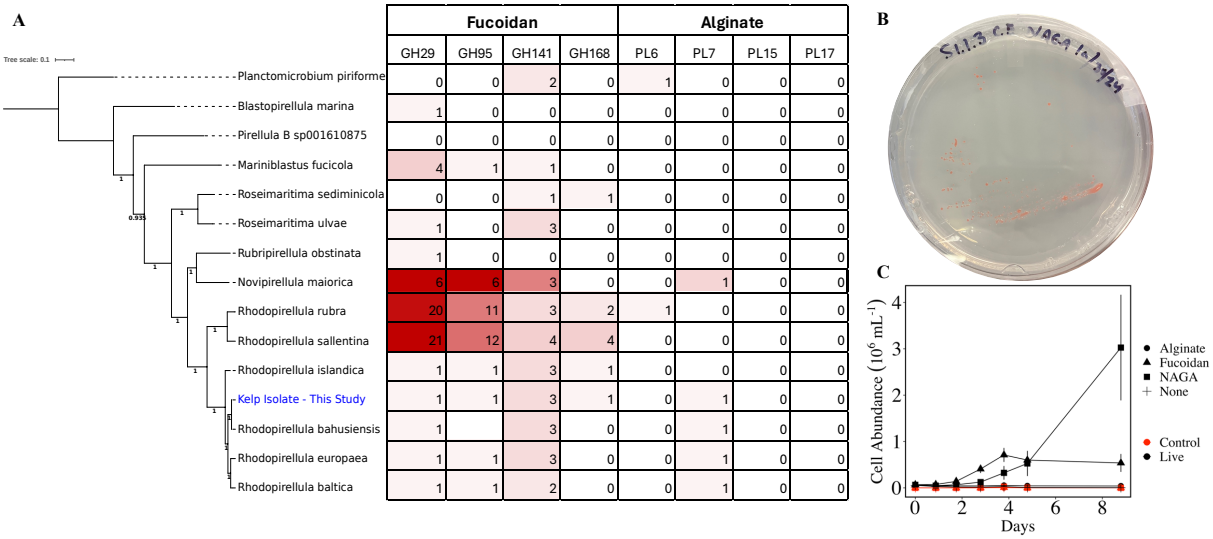

	Fucoidan				Alginate			
	GH29	GH95	GH141	GH168	PL6	PL7	PL15	PL17
Planctomicrobium piriforme	0	0	2	0	1	0	0	0
Blastopirellula marina	1	0	0	0	0	0	0	0
Pirellula B sp001610875	0	0	0	0	0	0	0	0
Mariniblastus fucicola	4	1	1	0	0	0	0	0
Roseimaritima sediminicola	0	0	1	1	0	0	0	0
Roseimaritima ulvae	1	0	3	0	0	0	0	0
Rubripirellula obstinata	1	0	0	0	0	0	0	0
Novipirellula maiorica	6	6	3	0	0	1	0	0
Rhodopirellula rubra	20	11	3	2	1	0	0	0
Rhodopirellula sallentina	21	12	4	4	0	0	0	0
Rhodopirellula islandica	1	1	3	1	0	0	0	0
Kelp Isolate - This Study	1	1	3	1	0	1	0	0
Rhodopirellula bahusiensis	1		3	0	0	1	0	0
Rhodopirellula europaea	1	1	3	0	0	1	0	0
Rhodopirellula baltica	1	1	2	0	0	1	0	0

Figure 6. The Planctomycetota family *Pirellulaceae* are fucoidan, not alginate consumers. (A) Phylogenetic tree of Planctomycetota isolates within the *Pirellulaceae* family. The isolated strain from this study is highlighted in blue text. The tree was rooted with one sequence from the Planctomycetota order Planctomycetales (family *Planctomycetaceae*), located at the top of the tree. Bootstrap scores are shown at the nodes. Paired with the phylogenetic position of each isolate are the number of glycoside hydrolases (GH29, GH95, GH141, GH168) and polysaccharide lyases (PL6, PL7, PL15, PL17) involved in fucoidan and alginate degradation, respectively, predicted in their genomes. **(B)** Isolation of *Rhodopirellula* sp. on an agar plate. **(C)** Isolate growth on model carbohydrates. Control incubations (red symbols) are sterile incubation media with all carbohydrate amendments (shapes). NAGA is *N*-acetyl glucosamine. Live incubations (black symbols) show the isolate's growth capability in response to amended carbohydrates. Points and error bars are the mean ±1 standard deviation cell abundance from triplicate incubations.

694 **References**

695 1. O'Callaghan M. Microbial inoculation of seed for improved crop performance: issues
696 and opportunities. *Appl Microbiol Biotechnol* 2016;**100**:5729–5746.
697 https://doi.org/10.1007/s00253-016-7590-9
698 2. Beijerinck M. Uber oligonitrophile mikroben. *Zentralbl Bakterol Parasitenkd Infekt Hyg*
699 *Abt II* 1901;**7**:561–582.
700 3. Burgunter-Delamare B et al. Metabolic Complementarity Between a Brown Alga and
701 Associated Cultivable Bacteria Provide Indications of Beneficial Interactions. *Front*
702 *Mar Sci* 2020;**7**. https://doi.org/10.3389/fmars.2020.00085
703 4. Somers E, Vanderleyden J, Srinivasan M. Rhizosphere Bacterial Signalling: A Love
704 Parade Beneath Our Feet. *Crit Rev Microbiol* 2004;**30**:205–240.
705 https://doi.org/10.1080/10408410490468786
706 5. Mannochio-Russo H et al. Microbiomes and metabolomes of dominant coral reef
707 primary producers illustrate a potential role for immunolipids in marine symbioses.
708 *Commun Biol* 2023;**6**:896. https://doi.org/10.1038/s42003-023-05230-1
709 6. Bakshani CR et al. Evolutionary conservation of the antimicrobial function of mucus: a
710 first defence against infection. *Npj Biofilms Microbiomes* 2018;**4**:14.
711 https://doi.org/10.1038/s41522-018-0057-2
712 7. Baker NR et al. Nutrient and moisture limitations reveal keystone metabolites linking
713 rhizosphere metabolomes and microbiomes. *Proc Natl Acad Sci* 2024;**121**.
714 https://doi.org/10.1073/pnas.2303439121

715 8. Zhalnina K et al. Dynamic root exudate chemistry and microbial substrate preferences
716 drive patterns in rhizosphere microbial community assembly. *Nat Microbiol*
717 2018;**3**:470–480. https://doi.org/10.1038/s41564-018-0129-3
718 9. Abdullah MI, Fredriksen S. Production, respiration and exudation of dissolved organic
719 matter by the kelp Laminaria hyperborea along the west coast of Norway. *J Mar Biol*
720 *Assoc U K* 2004;**84**:887–894. https://doi.org/10.1017/S002531540401015Xh
721 10. Myklestad SM. Dissolved Organic Carbon from Phytoplankton. In: Wangersky PJ (ed.),
722 Marine Chemistry. Berlin, Heidelberg: Springer Berlin Heidelberg, 2000, 111–148.
723 11. Davies PS. The role of zooxanthellae in the nutritional energy requirements of
724 Pocillopora eydouxi. *Coral Reefs* 1984;**2**:181–186.
725 https://doi.org/10.1007/BF00263571
726 12. Fogg GE. The Ecological Significance of Extracellular Products of Phytoplankton
727 Photosynthesis. 1983;**26**:3–14. https://doi.org/10.1515/botm.1983.26.1.3
728 13. Sogin EM et al. Sugars dominate the seagrass rhizosphere. *Nat Ecol Evol* 2022;**6**:866–
729 877. https://doi.org/10.1038/s41559-022-01740-z
730 14. Wild C et al. Coral mucus functions as an energy carrier and particle trap in the reef
731 ecosystem. *Nature* 2004;**428**:66–70. https://doi.org/10.1038/nature02344
732 15. Lee STM et al. Mucus Sugar Content Shapes the Bacterial Community Structure in
733 Thermally Stressed Acropora muricata. *Front Microbiol* 2016;**7**.
734 https://doi.org/10.3389/fmicb.2016.00371

16. Tremblay P et al. Mucus composition and bacterial communities associated with the tissue and skeleton of three scleractinian corals maintained under culture conditions. *J Mar Biol Assoc U K* 2011;**91**:649–657. https://doi.org/10.1017/S002531541000130X
17. Nelson CE et al. Coral and macroalgal exudates vary in neutral sugar composition and differentially enrich reef bacterioplankton lineages. *ISME J* 2013;**7**:962–979. https://doi.org/10.1038/ismej.2012.161
18. Thobor BM et al. Mucus carbohydrate composition correlates with scleractinian coral phylogeny. *Sci Rep* 2024;**14**:14019. https://doi.org/10.1038/s41598-024-64828-5
19. Krumhansl KA et al. Global patterns of kelp forest change over the past half-century. *Proc Natl Acad Sci* 2016;**113**:13785–13790. https://doi.org/10.1073/pnas.1606102113
20. Miller RJ et al. Giant kelp, Macrocystis pyrifera , increases faunal diversity through physical engineering. *Proc R Soc B Biol Sci* 2018;**285**:20172571. https://doi.org/10.1098/rspb.2017.2571
21. Eger AM et al. The value of ecosystem services in global marine kelp forests. *Nat Commun* 2023;**14**:1894. https://doi.org/10.1038/s41467-023-37385-0
22. Filbee-Dexter K et al. Carbon export from seaweed forests to deep ocean sinks. *Nat Geosci* 2024;**17**:552–559. https://doi.org/10.1038/s41561-024-01449-7
23. Krause-Jensen D, Duarte CM. Substantial role of macroalgae in marine carbon sequestration. *Nat Geosci* 2016;**9**:737–742. https://doi.org/10.1038/ngeo2790
24. Smith SV. Marine Macrophytes as a Global Carbon Sink. *Science* 1981;**211**:838–840. https://doi.org/10.1126/science.211.4484.838

25. Arafeh-Dalmau N et al. Marine heat waves threaten kelp forests. *Science* 2020;**367**:635–635. https://doi.org/10.1126/science.aba5244

26. Fredriksen S et al. Green gravel: a novel restoration tool to combat kelp forest decline. *Sci Rep* 2020;**10**:3983. https://doi.org/10.1038/s41598-020-60553-x

27. Duarte CM, Bruhn A, Krause-Jensen D. A seaweed aquaculture imperative to meet global sustainability targets. *Nat Sustain* 2022;**5**:185–193. https://doi.org/10.1038/s41893-021-00773-9

28. Bell TW et al. Geographical variability in the controls of giant kelp biomass dynamics. *J Biogeogr* 2015;**42**:2010–2021. https://doi.org/10.1111/jbi.12550

29. Bell TW, Siegel DA. Nutrient availability and senescence spatially structure the dynamics of a foundation species. *Proc Natl Acad Sci* 2022;**119**:e2105135118. https://doi.org/10.1073/pnas.2105135118

30. North WJ. Life-span of the Fronds of the Giant Kelp, Macrocystis pyrifera. *Nature* 1961;**190**:1214–1215. https://doi.org/10.1038/1901214a0

31. Reed DC, Rassweiler A, Arkema KK. Biomass Rather Than Growth Rate Determines Variation in Net Primary Production by Giant Kelp. *Ecology* 2008;**89**:2493–2505. https://doi.org/10.1890/07-1106.1

32. Gerard VA. Growth and utilization of internal nitrogen reserves by the giant kelp Macrocystis pyrifera in a low-nitrogen environment. *Mar Biol* 1982;**66**:27–35. https://doi.org/10.1007/BF00397251

33. Zhang Y et al. Adverse Environmental Perturbations May Threaten Kelp Farming Sustainability by Exacerbating Enterobacterales Diseases. *Environ Sci Technol* 2024;**58**:5796–5810. https://doi.org/10.1021/acs.est.3c09921

34. Ma M et al. Naturally occurring beneficial bacteria Vibrio alginolyticus X-2 protects seaweed from bleaching disease. *mBio* 2023;**14**:e00065-23. https://doi.org/10.1128/mbio.00065-23

35. James AK et al. Giant kelp microbiome altered in the presence of epiphytes. *Limnol Oceanogr Lett* 2020;**5**:354–362. https://doi.org/10.1002/lol2.10157

36. Michelou VK et al. The Ecology of Microbial Communities Associated with Macrocystis pyrifera. *PLOS ONE* 2013;**8**:e67480. https://doi.org/10.1371/journal.pone.0067480

37. Weigel BL, Pfister CA. Successional Dynamics and Seascape-Level Patterns of Microbial Communities on the Canopy-Forming Kelps Nereocystis luetkeana and Macrocystis pyrifera. *Front Microbiol* 2019;**10**. https://doi.org/10.3389/fmicb.2019.00346

38. Gao X et al. Adaptive traits of Planctomycetota bacteria to thrive in macroalgal habitats and establish mutually beneficial relationship with macroalgae. *Limnol Oceanogr Lett* 2024;**9**:745–753. https://doi.org/10.1002/lol2.10424

39. Weigel BL et al. Functional Insights into the Kelp Microbiome from Metagenome-Assembled Genomes. *mSystems* 2022;**7**:e01422-21. https://doi.org/10.1128/msystems.01422-21

40. Castro LC et al. Effect of marine heatwaves and warming on kelp microbiota influence trophic interactions. *Mol Ecol* 2024;**33**:e17267. https://doi.org/10.1111/mec.17267

41. Marzinelli EM et al. Continental-scale variation in seaweed host-associated bacterial communities is a function of host condition, not geography. *Environ Microbiol* 2015;**17**:4078–4088. https://doi.org/10.1111/1462-2920.12972

42. Qiu Z et al. Future climate change is predicted to affect the microbiome and condition of habitat-forming kelp. *Proc R Soc B Biol Sci* 2019;**286**:20181887. https://doi.org/10.1098/rspb.2018.1887

43. Florez JZ et al. Structure of the epiphytic bacterial communities of *Macrocystis pyrifera* in localities with contrasting nitrogen concentrations and temperature. *Algal Res* 2019;**44**:101706. https://doi.org/10.1016/j.algal.2019.101706

44. Xi T et al. The response mechanisms of kelp Macrocystis pyrifera holobiont to elevated temperature and CO2 concentration. *J Appl Phycol* 2025;**37**:1241–1251. https://doi.org/10.1007/s10811-024-03432-6

45. Zhang X et al. Chemical interactions between kelp Macrocystis pyrifera and symbiotic bacteria under elevated CO2 condition. *Mar Life Sci Technol* 2024;**6**:700–712. https://doi.org/10.1007/s42995-024-00259-5

46. Burgunter-Delamare B et al. Metabolic Complementarity Between a Brown Alga and Associated Cultivable Bacteria Provide Indications of Beneficial Interactions. *Front Mar Sci* 2020;**7**. https://doi.org/10.3389/fmars.2020.00085

47. Santa Barbara Coastal LTER, Reed DC. SBC LTER: Reef: Bottom Temperature: Continuous water temperature, ongoing since 2000. 2025. EDI, 2025.

48. Snyder JN et al. Sea Surface Temperature Imagery Elucidates Spatiotemporal Nutrient Patterns for Offshore Kelp Aquaculture Siting in the Southern California Bight. *Front Mar Sci* 2020;**7**. https://doi.org/10.3389/fmars.2020.00022
49. Halewood E et al. Determination of dissolved organic carbon and total dissolved nitrogen in seawater using High Temperature Combustion Analysis. *Front Mar Sci* 2022;**9**. https://doi.org/10.3389/fmars.2022.1061646
50. Engel A, Händel N. A novel protocol for determining the concentration and composition of sugars in particulate and in high molecular weight dissolved organic matter (HMW-DOM) in seawater. *Mar Chem* 2011;**127**:180–191. https://doi.org/10.1016/j.marchem.2011.09.004
51. Wada S et al. Quantitative and qualitative analyses of dissolved organic matter released from *Ecklonia cava* Kjellman, in Oura Bay, Shimoda, Izu Peninsula, Japan. *J Exp Mar Biol Ecol* 2007;**349**:344–358. https://doi.org/10.1016/j.jembe.2007.05.024
52. Buck-Wiese H et al. Fucoid brown algae inject fucoidan carbon into the ocean. *Proc Natl Acad Sci* 2023;**120**:e2210561119. https://doi.org/10.1073/pnas.2210561119
53. Oksanen J et al. vegan: Community Ecology Package. 2025. 2025.
54. Giovannoni SJ et al. 16S rRNA genes reveal stratified open ocean bacterioplankton populations related to the Green Non-Sulfur bacteria. *Proc Natl Acad Sci* 1996;**93**:7979–7984. https://doi.org/10.1073/pnas.93.15.7979
55. Apprill A et al. Minor revision to V4 region SSU rRNA 806R gene primer greatly increases detection of SAR11 bacterioplankton. *Aquat Microb Ecol* 2015;**75**:129–137. https://doi.org/10.3354/ame01753

841 56. Callahan BJ et al. DADA2: High-resolution sample inference from Illumina amplicon
842 data. *Nat Methods* 2016;**13**:581–583. https://doi.org/10.1038/nmeth.3869
843 57. Quast C et al. The SILVA ribosomal RNA gene database project: improved data
844 processing and web-based tools. *Nucleic Acids Res* 2012;**41**:D590–D596.
845 https://doi.org/10.1093/nar/gks1219
846 58. McMurdie PJ, Holmes S. Waste Not, Want Not: Why Rarefying Microbiome Data Is
847 Inadmissible. *PLOS Comput Biol* 2014;**10**:e1003531.
848 https://doi.org/10.1371/journal.pcbi.1003531
849 59. McMurdie PJ, Holmes S. phyloseq: An R Package for Reproducible Interactive Analysis
850 and Graphics of Microbiome Census Data. *PLOS ONE* 2013;**8**:e61217.
851 https://doi.org/10.1371/journal.pone.0061217
852 60. Love MI, Huber W, Anders S. Moderated estimation of fold change and dispersion for
853 RNA-seq data with DESeq2. *Genome Biol* 2014;**15**:550.
854 https://doi.org/10.1186/s13059-014-0550-8
855 61. Kolde R. pheatmap: Pretty Heatmaps. 2025. 2025.
856 62. Lage OM, Bondoso J. Bringing Planctomycetes into pure culture. *Front Microbiol*
857 2012;**3**. https://doi.org/10.3389/fmicb.2012.00405
858 63. Wiegand S et al. Cultivation and functional characterization of 79 planctomycetes
859 uncovers their unique biology. *Nat Microbiol* 2020;**5**:126–140.
860 https://doi.org/10.1038/s41564-019-0588-1

861 64. Chivian D et al. Metagenome-assembled genome extraction and analysis from
862 microbiomes using KBase. *Nat Protoc* 2023;**18**:208–238.
863 https://doi.org/10.1038/s41596-022-00747-x
864 65. Lee MD. GToTree: a user-friendly workflow for phylogenomics. *Bioinformatics*
865 2019;**35**:4162–4164. https://doi.org/10.1093/bioinformatics/btz188
866 66. Zhang H et al. dbCAN2: a meta server for automated carbohydrate-active enzyme
867 annotation. *Nucleic Acids Res* 2018;**46**:W95–W101.
868 https://doi.org/10.1093/nar/gky418
869 67. Eddy SR. Accelerated Profile HMM Searches. *PLOS Comput Biol* 2011;**7**:e1002195.
870 https://doi.org/10.1371/journal.pcbi.1002195
871 68. Blin K et al. antiSMASH 8.0: extended gene cluster detection capabilities and analyses
872 of chemistry, enzymology, and regulation. *Nucleic Acids Res* 2025;**53**:W32–W38.
873 https://doi.org/10.1093/nar/gkaf334
874 69. Patankar MS et al. A revised structure for fucoidan may explain some of its biological
875 activities. *J Biol Chem* 1993;**268**:21770–21776. https://doi.org/10.1016/S0021-
876 9258(20)80609-7
877 70. Sichert A et al. Ion-exchange purification and structural characterization of five
878 sulfated fucoidans from brown algae. *Glycobiology* 2021;**31**:352–357.
879 https://doi.org/10.1093/glycob/cwaa064
880 71. Brzezinksi M et al. Multiple Sources and Forms of Nitrogen Sustain Year-Round Kelp
881 Growth on the Inner Continental Shelf of the Santa Barbara Channel. *Oceanography*
882 2013;**26**:114–123. https://doi.org/10.5670/oceanog.2013.53

883 72. Reed D, Miller R. SBC LTER: Reef: Macrocystis pyrifera CHN content (carbon,
884 hydrogen, nitrogen), ongoing since 2002 ver 21. 2025. EDI, 2025.
885 73. Rodriguez GE et al. The importance of progressive senescence in the biomass
886 dynamics of giant kelp (Macrocystis pyrifera). *Ecology* 2013;**94**:1848–1858.
887 https://doi.org/10.1890/12-1340.1
888 74. Bengtsson MM et al. Bacterial diversity in relation to secondary production and
889 succession on surfaces of the kelp Laminaria hyperborea. *ISME J* 2012;**6**:2188–2198.
890 https://doi.org/10.1038/ismej.2012.67
891 75. Minich JJ et al. Elevated temperature drives kelp microbiome dysbiosis, while elevated
892 carbon dioxide induces water microbiome disruption. *PLOS ONE* 2018;**13**:e0192772.
893 https://doi.org/10.1371/journal.pone.0192772
894 76. Song W et al. Contribution of horizontal gene transfer to the functionality of microbial
895 biofilm on a macroalgae. *ISME J* 2021;**15**:807–817. https://doi.org/10.1038/s41396-
896 020-00815-8
897 77. Mann KH. Seaweeds: Their Productivity and Strategy for Growth: The role of large
898 marine algae in coastal productivity is far more important than has been suspected.
899 *Science* 1973;**182**:975–981. https://doi.org/10.1126/science.182.4116.975
900 78. Bakshani CR et al. Carbohydrate-active enzymes from Akkermansia muciniphila
901 break down mucin O-glycans to completion. *Nat Microbiol* 2025;**10**:585–598.
902 https://doi.org/10.1038/s41564-024-01911-7

903 79. Guo S et al. Structural Basis of Ligand Selectivity by a Bacterial Adhesin Lectin
904 Involved in Multispecies Biofilm Formation. *mBio* 2021;**12**:10.1128/mbio.00130-21.
905 https://doi.org/10.1128/mbio.00130-21
906 80. Sicard J-F et al. N-Acetyl-glucosamine influences the biofilm formation of Escherichia
907 coli. *Gut Pathog* 2018;**10**:26. https://doi.org/10.1186/s13099-018-0252-y
908 81. Callow ME, Evans LV. Localization of sulphated polysaccharides by X-ray
909 microanalysis in Laminaria saccharina. *Planta* 1976;**131**:155–157.
910 https://doi.org/10.1007/BF00389988
911 82. Evans LV, Simpson M, Callow ME. Sulphated polysaccharide synthesis in brown
912 algae. *Planta* 1973;**110**:237–252. https://doi.org/10.1007/BF00387636
913 83. Fitton JH, Stringer DN, Karpiniec SS. Therapies from Fucoidan: An Update. *Mar Drugs*
914 2015;**13**:5920–5946. https://doi.org/10.3390/md13095920
915 84. Sichert A et al. Verrucomicrobia use hundreds of enzymes to digest the algal
916 polysaccharide fucoidan. *Nat Microbiol* 2020;**5**:1026–1039.
917 https://doi.org/10.1038/s41564-020-0720-2
918 85. Kloareg B, Quatrano RS. Structure of the cell walls of marine algae and
919 ecophysiological functions of the matrix polysaccharides. *Oceanogr Mar Biol Annu*
920 *Rev* 1988;**26**:259–315.
921 86. Thomas F et al. Isotopic tracing reveals single-cell assimilation of a macroalgal
922 polysaccharide by a few marine Flavobacteria and Gammaproteobacteria. *ISME J*
923 2021;**15**:3062–3075. https://doi.org/10.1038/s41396-021-00987-x

87. Zhang Y-S et al. Metagenomic insights into the dynamic degradation of brown algal polysaccharides by kelp-associated microbiota. *Appl Environ Microbiol* 2024;**90**:e02025-23. https://doi.org/10.1128/aem.02025-23

88. Lin JD, Lemay MA, Parfrey LW. Diverse Bacteria Utilize Alginate Within the Microbiome of the Giant Kelp Macrocystis pyrifera. *Front Microbiol* 2018;**9**:1914. https://doi.org/10.3389/fmicb.2018.01914

89. Fernández-Gómez B et al. Ecology of marine Bacteroidetes: a comparative genomics approach. *ISME J* 2013;**7**:1026–1037. https://doi.org/10.1038/ismej.2012.169

90. English CJ et al. Senescence-driven solubilization of biomass is the main source of kelp-derived dissolved organic carbon to the coastal ocean. *Commun Biol* 2025;**8**:1172. https://doi.org/10.1038/s42003-025-08477-y

91. Hehemann J-H et al. Adaptive radiation by waves of gene transfer leads to fine-scale resource partitioning in marine microbes. *Nat Commun* 2016;**7**:12860. https://doi.org/10.1038/ncomms12860

92. Kikuzawa K. A Cost-Benefit Analysis of Leaf Habit and Leaf Longevity of Trees and Their Geographical Pattern. *Am Nat* 1991;**138**:1250–1263. https://doi.org/10.1086/285281

93. Lewis AL, Kohler JJ, Aebi M. Microbial Lectins: Hemagglutinins, Adhesins, and Toxins. In: Varki A et al. (eds), Essentials of Glycobiology, 4th edn. Cold Spring Harbor (NY): Cold Spring Harbor Laboratory Press, 2022, 505–516.

94. Vidal-Melgosa S et al. Diatom fucan polysaccharide precipitates carbon during algal blooms. *Nat Commun* 2021;**12**:1150. https://doi.org/10.1038/s41467-021-21009-6

946 95. Teeling H et al. Substrate-Controlled Succession of Marine Bacterioplankton
947 Populations Induced by a Phytoplankton Bloom. *Science* 2012;**336**:608–611.
948 https://doi.org/10.1126/science.1218344
949 96. Kallscheuer N et al. The planctomycete Stieleria maiorica Mal15T employs
950 stieleriacines to alter the species composition in marine biofilms. *Commun Biol*
951 2020;**3**:303. https://doi.org/10.1038/s42003-020-0993-2
952 97. Riemann L, Azam F. Widespread N-Acetyl-d-Glucosamine Uptake among Pelagic
953 Marine Bacteria and Its Ecological Implications. *Appl Environ Microbiol* 2002;**68**:5554–
954 5562. https://doi.org/10.1128/AEM.68.11.5554-5562.2002
955 98. Rabus R et al. Analysis of N-acetylglucosamine metabolism in the marine bacterium
956 Pirellula sp. strain 1 by a proteomic approach. *Proteomics* 2002;**2**:649–655.
957 https://doi.org/10.1002/1615-9861(200206)2:6<649::AID-PROT649>3.0.CO;2-R
958 99. Jeske O et al. Developing Techniques for the Utilization of Planctomycetes As
959 Producers of Bioactive Molecules. *Front Microbiol* 2016;**7**.
960 https://doi.org/10.3389/fmicb.2016.01242
961 100. Lage OM, Bondoso J. Planctomycetes and macroalgae, a striking association. *Front*
962 *Microbiol* 2014;**5**. https://doi.org/10.3389/fmicb.2014.00267
963 101. Pérez-Cruz C et al. Mechanisms of recalcitrant fucoidan breakdown in marine
964 Planctomycetota. *Nat Commun* 2024;**15**:10906. https://doi.org/10.1038/s41467-024-
965 55268-w
966 102. Sogin EM et al. Sugars dominate the seagrass rhizosphere. *Nat Ecol Evol* 2022;**6**:866–
967 877. https://doi.org/10.1038/s41559-022-01740-z

103. Bais HP et al. THE ROLE OF ROOT EXUDATES IN RHIZOSPHERE INTERACTIONS WITH PLANTS AND OTHER ORGANISMS. *Annu Rev Plant Biol* 2006;**57**:233–266. https://doi.org/10.1146/annurev.arplant.57.032905.105159

104. Sasse J, Martinoia E, Northen T. Feed Your Friends: Do Plant Exudates Shape the Root Microbiome? *Trends Plant Sci* 2018;**23**:25–41. https://doi.org/10.1016/j.tplants.2017.09.003

Supplementals

Supplemental Table 1: ANOVA results for differences in relative abundance of top 10 families btween mature and developmental stages shown in Figure 4. Significant results means the observed relative abundances of the family was higher in in the mature developmental stage

family	term	df	sumsq	meansq	statistic	p.value	adjusted_p.value
Granulosicoccaceae	phys_state	1	0.38	0.38	20.47	3.65E-05	3.65E-04
Thiotrichaceae	phys_state	1	0.03	0.03	2.82	0.100	0.144
Pirellulaceae	phys_state	1	0.07	0.07	17.75	1.01E-04	5.03E-04
Cellvibrionaceae	phys_state	1	0.00	0.00	0.23	0.638	0.638
Flavobacteriaceae	phys_state	1	0.04	0.04	17.37	1.71E-04	5.71E-04
Hyphomonadaceae	phys_state	1	0.01	0.01	7.99	0.007	0.011
Saprospiraceae	phys_state	1	0.00	0.00	1.21	0.277	0.344
Microtrichaceae	phys_state	1	0.00	0.00	1.06	0.309	0.344
Rhodobacteraceae	phys_state	1	0.01	0.01	16.11	2.71E-04	6.78E-04
Arenicellaceae	phys_state	1	0.01	0.01	15.72	4.03E-04	8.06E-04

Supplemental Table 2: ANOVA results for differences in relative abundance of top 10 families between spring and summer cohorts shown in Supplemental Figure 6.Significant results means the observed relative abundances of the family was higher in the spring.

family	term	df	sumsq	meansq	statistic	p.value	adjusted_p.value
Granulosicoccaceae	season	1	0.045	0.045	1.79	0.1870	0.255150
Thiotrichaceae	season	1	0.009	0.009	0.90	0.3487	0.387435
Pirellulaceae	season	1	0.009	0.009	1.92	0.1721	0.255150
Cellvibrionaceae	season	1	0.006	0.006	1.73	0.2041	0.255150
Flavobacteriaceae	season	1	0.036	0.036	14.10	0.0006	0.001930
Hyphomonadaceae	season	1	0.000	0.000	0.08	0.7820	0.781972
Saprospiraceae	season	1	0.056	0.056	52.15	0.0000	0.000000
Microtrichaceae	season	1	0.037	0.037	20.60	0.0000	0.000203
Rhodobacteraceae	season	1	0.007	0.007	10.69	0.0023	0.005728
Arenicellaceae	season	1	0.002	0.002	1.71	0.2005	0.255150

Supplemental Table 3. Spearman's rank correlation rho and FDR-adjusted p-values for abundant ASVs and sugar mole% in Cluster A (Figure 5A).

Sugar	Pirellulaceae_Blastopirellula_NA_12	Pirellulaceae_Blastopirellula_NA_7	Granulosicoccaceae_Granulosicoccus_NA_11	Pirellulaceae_Blastopirellula_NA_11	Granulosicoccaceae_Granulosicoccus_NA_6	Saprospiraceae_Portibacter_NA_5
Fucose	0.42,0.04001	0.28,0.23828	0.58,0.00137	0.58,0.00131	0.48,0.01154	0.11,0.72229
Rhamnose	-0.13,0.65786	-0.24,0.31968	-0.08,0.7988	-0.1,0.74709	0.11,0.70898	0.06,0.85406
Galactosamine	0.02,0.95119	0.11,0.72086	0.19,0.45915	0.33,0.13624	-0.08,0.7946	0.52,0.00553
Arabinose	-0.2,0.44136	0,0.9889	-0.08,0.79993	0.01,0.97272	-0.29,0.19491	0.34,0.12517
Glucosamine	0.61,0.00082	0.62,0.00072	0.54,0.00364	0.55,0.00294	0.31,0.16831	0.18,0.50321
Galactose	-0.01,0.97369	-0.09,0.77111	0.2,0.41287	0.03,0.92888	0.32,0.14726	0,0.99919
Gal-URA	-0.14,0.62703	-0.03,0.93147	-0.17,0.53314	-0.06,0.84141	0.03,0.92321	0.04,0.91045
Glc-URA	-0.05,0.8645	0.06,0.83048	-0.1,0.73885	0.04,0.90437	-0.13,0.6549	0.18,0.47232
Man-URA	-0.38,0.08039	-0.25,0.3076	-0.51,0.00716	-0.56,0.00232	-0.56,0.00236	-0.24,0.31968

Supplemental Table 4. Spearman's rank correlation rho and FDR-adjusted p-value for abundant ASVs and sugar mole% in Cluster B (Figure 5A).

Sugar	Thiotrichaceae_Leucothrix_NA_8	Microtrichaceae_Sva0996 marine group_NA_8	Trueperaceae_Truepera_NA_1	Microtrichaceae_Sva0996 marine group_NA_1	Cellvibrionaceae_NA_NA_6	Flavobacteriaceae_Ulvibacter_NA_2	Granulosicoccaceae_Granulosicoccus_NA_8	Arenicellaceae_Arenicella_NA_6	Arenicellaceae_Arenicella_NA_3	Flavobacteriaceae_Algitalea_NA	Microtrichaceae_Sva0996 marine group_NA_7
Fucose	-0.6, 0.00103	-0.59, 0.00127	-0.62, 0.00072	-0.57, 0.00183	-0.62, 0.00072	-0.65, 0.00062	-0.56, 0.00204	-0.48, 0.01154	-0.52, 0.00592	-0.45, 0.02168	-0.4, 0.05822
Rhamnose	-0.16, 0.56818	-0.18, 0.48463	0.04, 0.90403	0.08, 0.7963	-0.01, 0.97369	-0.06, 0.83943	-0.09, 0.77111	0.04, 0.90403	0.04, 0.88867	0.07, 0.82261	0.1, 0.74264
Galactosamine	-0.16, 0.56818	-0.24, 0.33629	-0.22, 0.39835	-0.24, 0.32614	-0.39, 0.06541	-0.5, 0.00812	-0.07, 0.80713	-0.36, 0.10322	-0.39, 0.06515	-0.49, 0.0094	-0.35, 0.11039
Arabinose	-0.01, 0.98342	0.1, 0.74264	0.11, 0.72229	0.06, 0.8338	-0.15, 0.60259	-0.2, 0.44136	-0.03, 0.93147	-0.21, 0.41287	-0.1, 0.73885	-0.23, 0.36489	-0.17, 0.50885
Glucosamine	-0.53, 0.00428	-0.31, 0.17494	-0.51, 0.00687	-0.52, 0.00617	-0.49, 0.01013	-0.51, 0.00716	-0.21, 0.41287	-0.61, 0.00074	-0.6, 0.00094	-0.55, 0.00294	-0.62, 0.00072
Galactose	-0.32, 0.15322	-0.33, 0.13215	-0.28, 0.23744	-0.22, 0.37359	-0.25, 0.31968	-0.26, 0.28245	-0.47, 0.01436	-0.05, 0.86412	-0.03, 0.94058	-0.13, 0.64198	0.08, 0.79993
Gal-URA	0.07, 0.82261	0.08, 0.7988	0.11, 0.69992	0.08, 0.80234	0.13, 0.65786	0.12, 0.69992	-0.09, 0.76834	0.1, 0.74085	0.19, 0.45589	0.12, 0.69874	0.19, 0.44427
Glc-URA	0.21, 0.41287	0.13, 0.65786	0.16, 0.56818	0.07, 0.82261	-0.01, 0.97369	-0.01, 0.98111	0.18, 0.47232	-0.08, 0.79672	-0.07, 0.82575	-0.12, 0.6634	-0.24, 0.33247
Man-URA	0.65, 0.00062	0.62, 0.00072	0.55, 0.00294	0.5, 0.00805	0.59, 0.00127	0.64, 0.00062	0.57, 0.00183	0.51, 0.00716	0.54, 0.00383	0.48, 0.01154	0.35, 0.11039

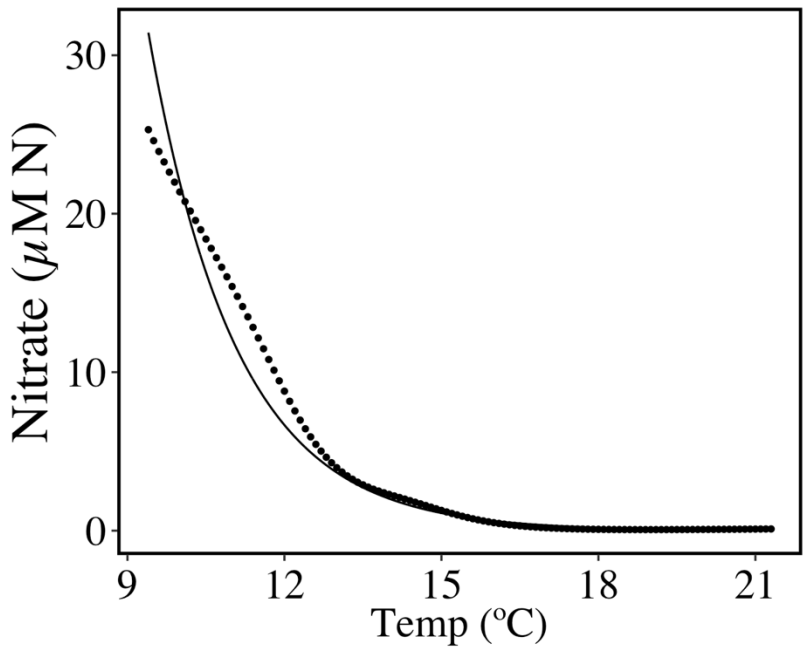

Supplemental Figure 1. Temperature to nitrate relationship for inshore water in the Santa Barbara Channel. Points are from the T2N look up table compiled by Snyder et al. 2020 . Solid line is the exponential regression used to calculate nitrate at Mohawk Reef at our study site: Nitrate (μM N) $= 8565.5 * e^{(-0.597*\text{Temp}(^{o}\text{C}))}$, $R^2 = 0.95$.

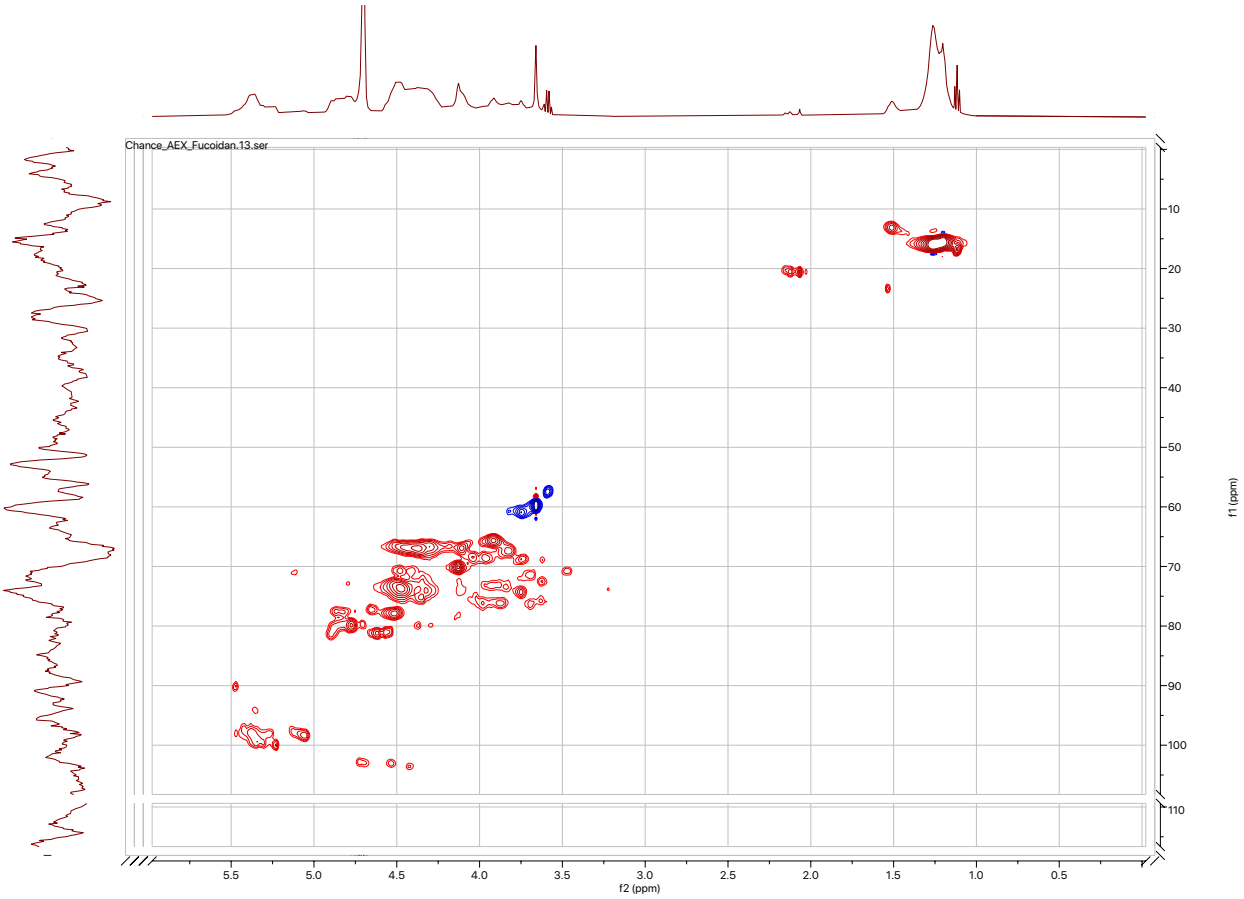

Supplemental Figure 2. ^{1}H-^{13}C HSQC NMR spectrum of IEX purified fucoidan from *Macrocystis pyrifera*. Correlations showing carbons with an even number of protons are blue and those with an odd number of protons are shown in red.

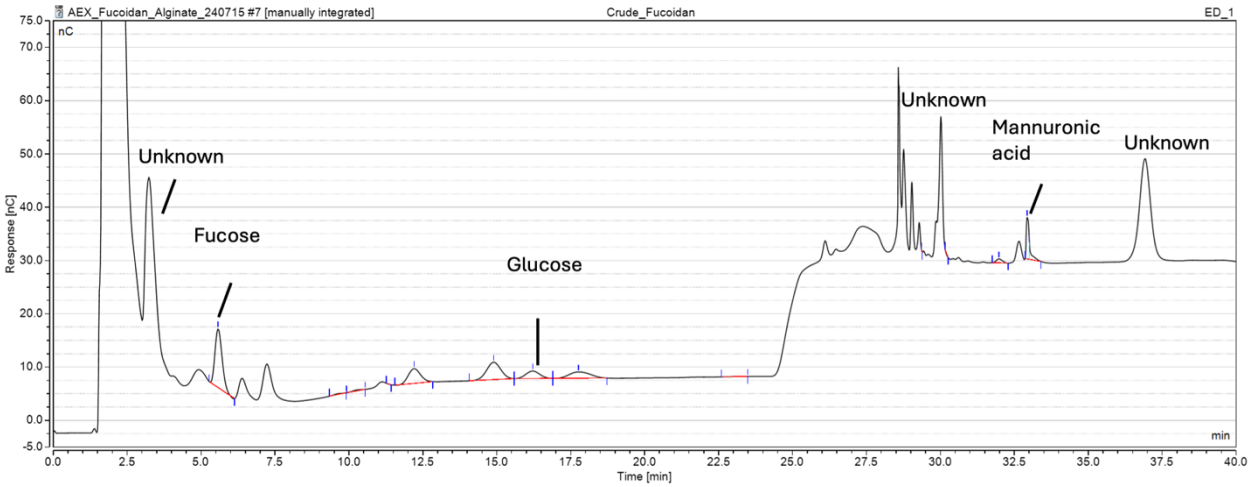

Supplemental Figure 3. HPAEC-PAD chromatogram of crude fucoidan from supplier. Note that peak area for fucose is relatively equal to areas from sugars not found in fucoidan (glucose, mannuronic acid) compared to fucose in IEX-purified fucoidan (Supplemental Figure 4). Also, there are large contributions from unknown peaks, possibly contaminating sugars in the sugar alcohol range (0 - 5 minutes) and acidic sugar range (30 - 40 minutes).

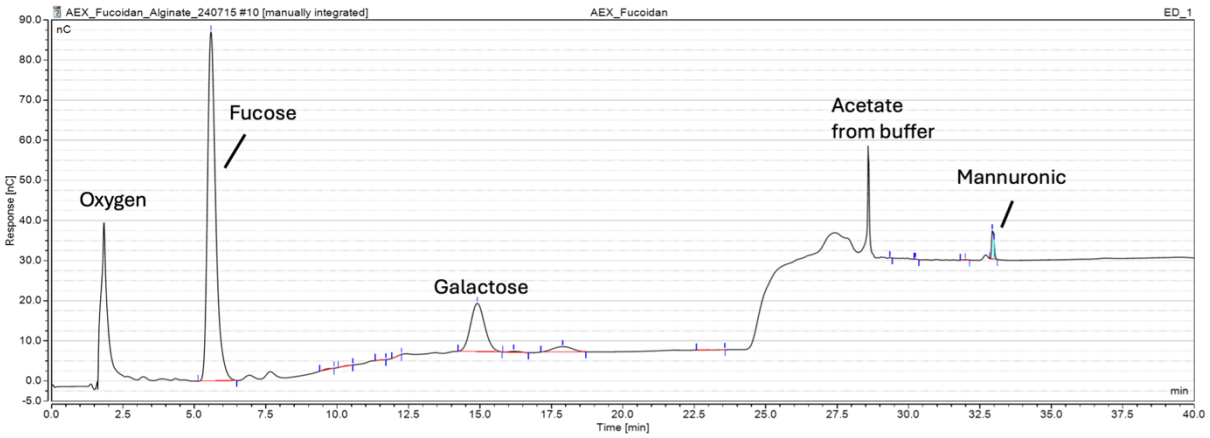

Supplemental Figure 4. HPAEC-PAD chromatogram of IEX purified fucoidan. Note that peak area of fucose enhanced compared to small remaining contaminating sugars (mannuronic acid) compared to Supplemental Figure 3. Contribution of galactose indicates fucoidan from *M. pyrifera* is likely a heterofucan. The two prominent peaks at the beginning and middle of the chromatogram are from dissolved oxygen and acetate from the sample and elution buffer, respectively.

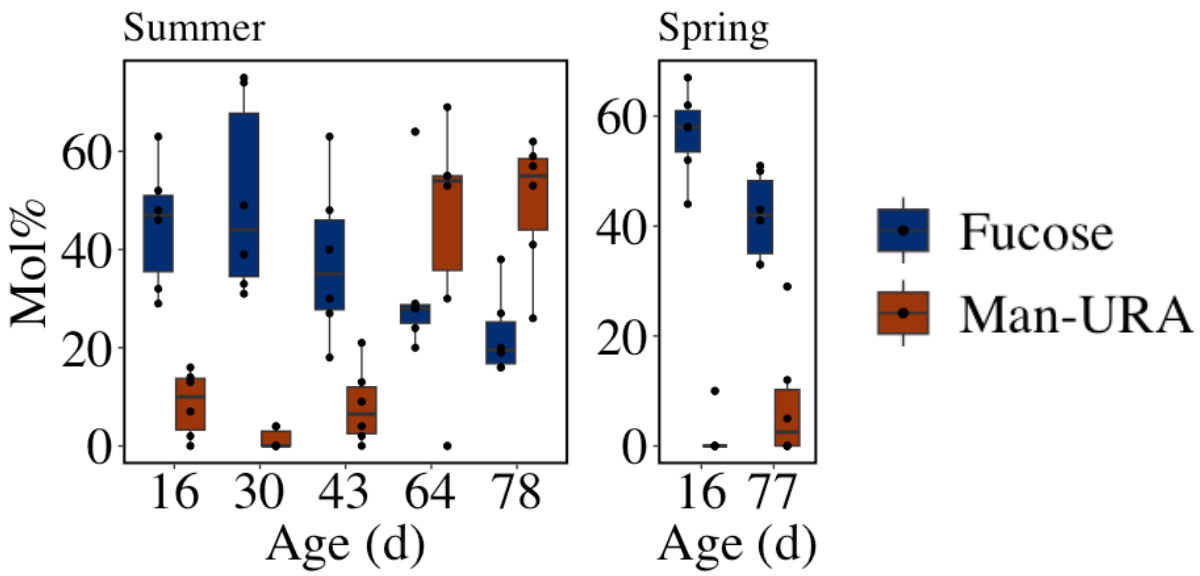

Supplemental Figure 5: Mole% of fucose and mannuronic acid (Man-URA) across age and and seasons. (A) Summer (B) Spring. The top and bottom border of each box represent the 25th and 75th percentiles, the horizontal line inside each box represents the median and the whiskers represent 1.5*IQR. Outliers are shown by points beyond the whiskers.

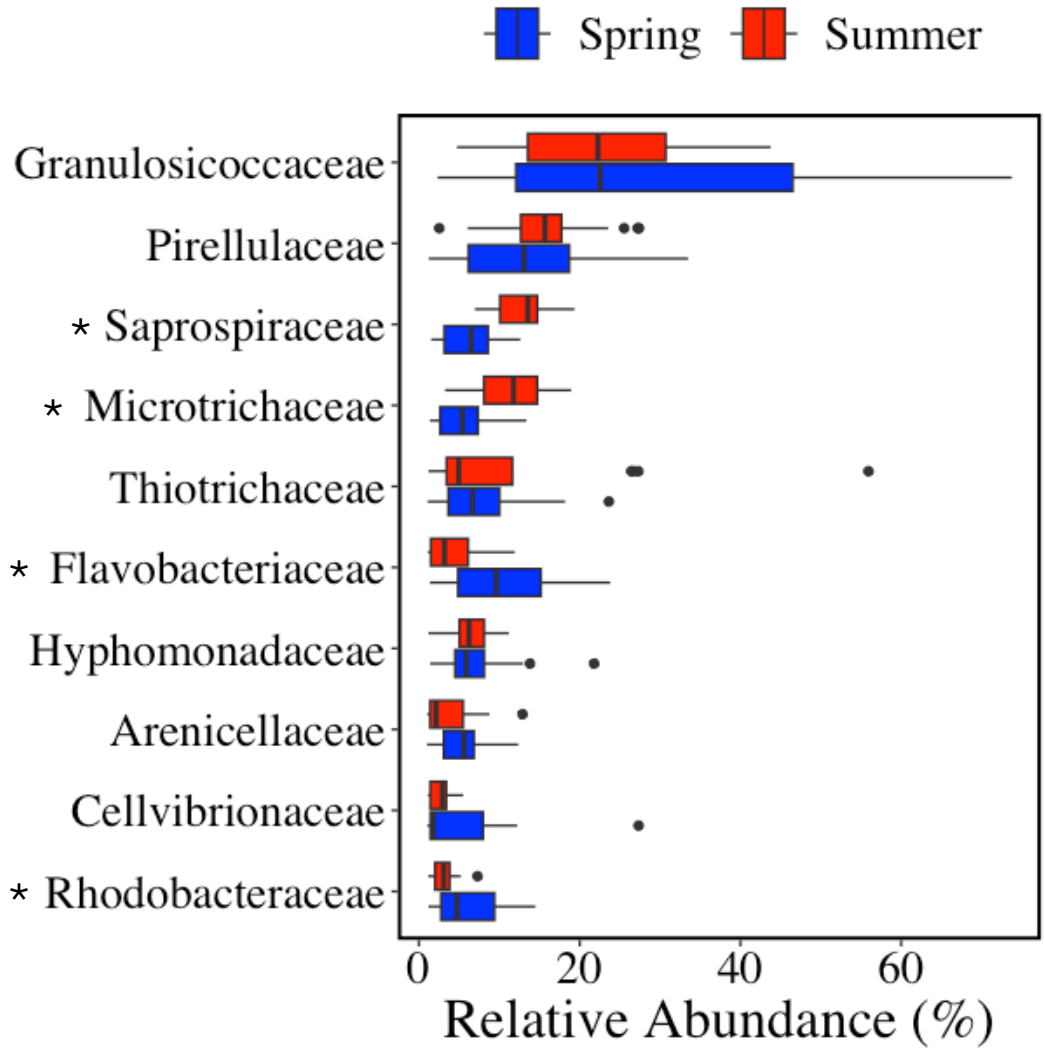

Supplemental Figure 6: **Relative abundance of bacterial clades at the family level on the surface of giant kelp blades between the spring and summer periods**. Shown are the top 10 families with a collective relative abundance > 1% during either season. The left and right border of each box represent the 25th and 75th percentiles, the vertical line inside each box represents the median and the whiskers represent 1.5*IQR. Outliers are shown by points beyond the whiskers. Asterisks next to family names indicate significant differences in the relative abundances between seasons (ANOVA, FDR-adjusted p-value < 0.05).

PKS:

Overview 1.1 1.2 2.1 5.1 6.1 6.2 11.1 14.1 19.1 21.1 24.1

Identified secondary metabolite regions using strictness 'relaxed'

Region	Type	From	To	Similarity Confidence	Most similar known cluster	
Region 1.1	terpene	26,265	47,299			
Region 1.2	T1PKS	384,091	432,847			
Region 2.1	NRPS, T1PKS	53,796	104,796			
Region 5.1	NRPS-like	255,744	298,524			
Region 6.1	terpene-precursor	208,364	229,317			
Region 6.2	NRPS-like	243,654	285,996			
Region 11.1	terpene	97,632	121,599			
Region 14.1	NRPS-like	32,425	76,012	High	3,5-dibromo-p-anisic acid	other:other
Region 19.1	T1PKS	73,119	120,375			
Region 21.1	terpene	1	20,499			
Region 24.1	T3PKS	88,940	130,043			

Supplemental Figure 7: AntiSMASH analysis results of the *Rhodopirellula sp* isolate genome.